Ionized Gas in Active Galactic Nuclei

Hagai Netzer

School of Physics and Astronomy
Tel Aviv University

Abstract

This review gives an introduction to the physics of ionized gas in active galactic nuclei (AGN). The main topics are: Definition of the AGN phenomenon, methods for discovering AGN, basic AGN observations, photoionization and recombination of low density plasma, energy balance and gas temperature, the spectrum of ionized gas, dust and reddening, the motion of ionized gas under the influence of strong radiation fields, the broad line region (BLR), the narrow line region (NLR), and the highly ionized outflowing gas in AGN.

Key words: ionized gas, ionization, recombination, collisions, emission lines, optical depth, broad line region, narrow line region, highly ionized gas,

1 Basic observations of Active Galactic Nuclei

The only name that is used in this review is AGN. An object will be considered an AGN if at least one of the following is fulfilled:

(1) It contains a compact nuclear region emitting a significant fraction of the total energy, much beyond what is expected from stellar processes typical of this type of galaxies.
(2) It exhibits the clear signature of continuum emission produced by non-stellar processes.
(3) Its spectrum contains strong emission lines indicating non-stellar excitation processes.
(4) It shows line and/or continuum variations.

This is a very broad definition that, in some cases, extends the limits and overlap with sources that are not associated with accreting BHs. An object can leave the AGN category if its luminosity is reduced below a certain limit and new AGN can "appear" occasionally when a non-active source undergoes a sudden burst of activity. Sub-categories of the AGN family may be related

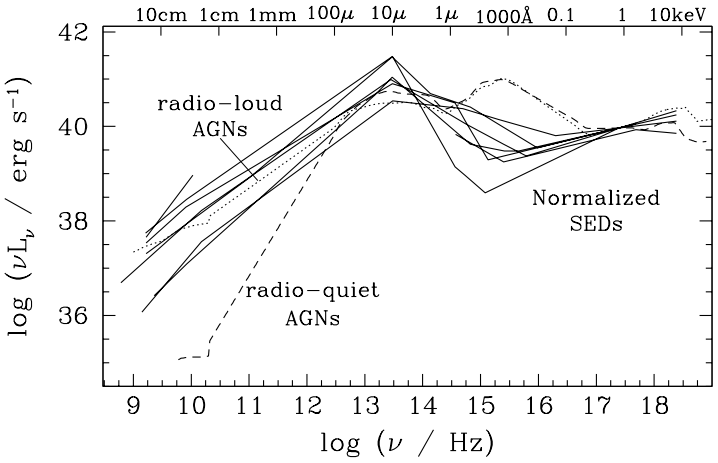

Fig. 1. Broad band spectral energy distribution (SED) for various types AGN (courtesy of L. Ho)

to the radio properties, to the emission line widths, to obscuration, viewing angles and the level of variability.

1.1 The spectral energy distribution of AGN

The spectral energy distribution (SED) of AGN has been studied in numerous sources and in various energy bands. Fig. 1.1 shows some examples covering the range of $10^9 - 10^{18}$ Hz and comparing sources with various luminosities and spectral shapes. All quantities related to the SED are described by either L_ν (erg s^{-1} Hz^{-1}) or L_λ (erg s^{-1} λ^{-1}). The conversion between the two is obtained from a simple energy conservation argument, $L_\nu d\nu = L_\lambda d\lambda$.

1.2 The optical-UV spectrum of AGN

The optical-ultraviolet (UV) spectrum of AGN shows many prominent emission lines that are the source for understanding many of the important properties of such objects. The relative line intensities provide information about the gas density and temperature, the gas composition, column density and degree of obscuration of the central source. The line profiles are used to deduce the gas dynamics and the emission line variations are the most reliable, perhaps only source for directly measure the central black hole (BH) mass. These topics are discussed later in this review and in several contributions by

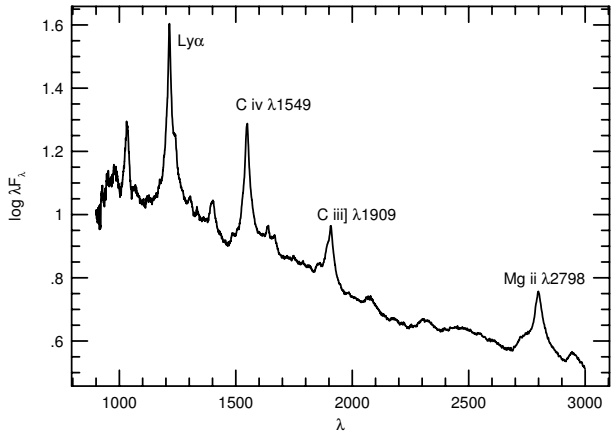

Fig. 2. A composite spectrum of high luminosity type-I AGN

others. Fig. 1.2 is an example of a composite spectrum obtained by combining many spectra of luminous AGN at various redshifts.

1.3 AGN Variability

This is another important characteristic of AGN which will be discussed in several other contributions. Variability of type-I AGN is observed in all parts of the spectrum, from radio waves to X-rays and even γ-rays. The various bands are probably related although not necessarily in a simple and direct way. Thus, X-ray variations are likely to be the result of accretion disk instabilities and radio variability, in radio-loud sources, arise, probably, from jet-related processes. Fig. 1.3 shows a typical example. The source in question is NGC 3783 and the light curves shown represent several days of observations by *Chandra*.

While the general topic of AGN variability will not be discussed in this review, it is important to note that typical variability time scales, and variability amplitudes, seem to be inversely correlated with source luminosity, perhaps through the accretion rate onto the central BH. This is clearly seen in the X-ray and optical bands, where most such studies have been conducted, with indications in other spectral bands as well.

1.4 Discovering AGN

There are various methods for discovering AGN, some almost as old as the subject itself (mid-1960s). The more recent methods are the ones that resulted

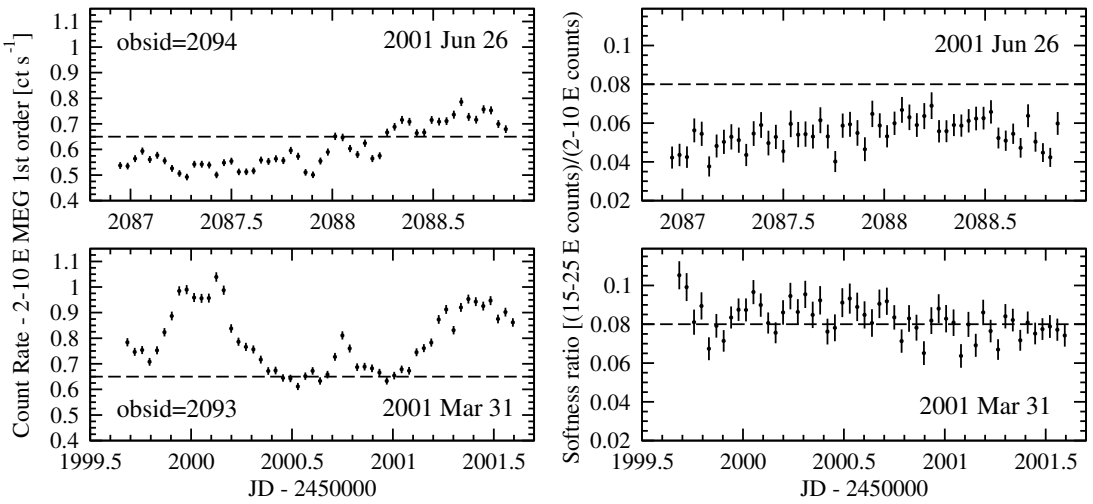

Fig. 3. Two 2001 light curves of NGC 3783 as observed by *Chandra*. The left hand side shows count rates in the 2–10 keV range and the right hand side gives the "hardness ratio" which is obtained by dividing count rates in the two energy bands specified on the vertical axis of the diagram.

in the largest number of sources and the most significant statistics. The most important methods are:

(1) By the color of their SED. There are several detection methods based on a combination of optical colors from 3 to 5 optical bands. Such methods clearly separate the non-thermal component of the SED (in comparison with the black-body type stellar SED). The most advanced of those, like the Sloan Digital Sky Survey (SDSS) use 5 optical bands that are also efficient in discovering high redshift sources by detecting the reduced emitted flux belong the Lyman edge. Such studies are supplemented, now-a-days, with 3–4 infrared (IR) colors.

(2) By their radio properties. About 10% of all AGN are radio loud and hence can be found by correlating their radio and optical positions. Various techniques, at different radio frequencies, can be use to separate steep from flat spectrum radio sources and discover the active nucleus in type-II AGN.

(3) By their optical spectrum. Discovering AGN directly by their spectrum, mostly by the large contrast between the strong broad emission and absorption lines and the underlying continuum, was a very useful method in the 1970s. It produced the first large AGN samples that were then used to characterize the population properties. The method is based on objective prism surveys, which were eventually supplemented by high-

resolution follow-up spectroscopy. The method is very inefficient in discovering type-II AGN.

(4) By their X-ray properties: Almost all AGN are strong X-ray emitters. This can be used to discover AGN in deep X-ray images. The first large X-ray detected samples were the result of *ROSAT* observations. More recently (since 1999) there are several very deep *Chandra* and *XMM-Newton* surveys that are being added to the list. Needless to say, optical follow-up spectroscopy is needed to confirm those detections. X-ray selected AGN samples are not efficient in discovering very high redshift AGN because of the limited sensitivity of the X-ray instruments.

(5) By their variability: This is an interesting method that has not been used, very much, because of various experimental limitations. It requires at least two visits per field and follow-up spectroscopy.

(6) By their IR properties: Several recent IR surveys, most notably by *Spitzer*, have been used to discover AGN with unusual IR properties (e.g. by their 24μm flux).

The result of all such surveys are more than 10^5 known AGN where the number is increasing very fast. Some abbreviations of the best known large surveys are: SDSS, 2dF, 2SLAQ, LAS, HDFS and HDFN.

1.5 AGN terminology

The study of AGN has produced many terms and abbreviations. Only the most common ones will be used in this review, e.g., the narrow line region (NLR), the broad line region (BLR), the highly ionized gas (HIG) and the black hole (BH). The terms "type-I AGN" (those objects showing broad, strong optical-UV emission lines in their spectrum) and "type-II AGN" (those showing prominent narrow emission lines, very faint, if any, broad lines, and a large X-ray obscuring column), are used to classify all sources into only two major sub-groups. Given this division we note that some type-I or type-II sources can be strong or weak radio emitters, strong or weak X-ray emitters, etc.

2 Physical processes in AGN gas

Ionized AGN gas is found from very close to the central BH, at $r \simeq 1000 r_g$, where $r_g = GM/c^2$, to distances of several kpc. This gas is exposed to the strong central radiation field and its properties are well described by considering photoionization and recombination and neglecting most other ionization and excitation processes. Notable exceptions are regions of violent star formation where mechanical heating and ionization, due to super-novae explosions

and fast stellar winds, are major sources of energy input to the gas. The spectrum of such regions is typical of thermal plasma although photoionization can be important too.

This section explains the general principles needed for understanding the emission line spectrum of active galaxies and the most important physical processes necessary to model their spectrum. The main underlying assumption is that the gas density is low enough, $N_H < 10^{12}$ cm^{-3}, that collisional transitions among excited states are of secondary importance for most ions, except for hydrogen and helium.

2.1 Photoionization and radiative recombination

Consider gas at a distance r from a point source of total luminosity L and monochromatic luminosity L_ν. The fractional ionization of ion X is determined by the ionization rate, per particle, due to flux reaching the location of the ion, I_X, and by the recombination rate per particle, R_X.

Assume σ_ν is the photoionization cross section of ion X from its threshold ionization ν_X (normally the ground level), $\alpha_X(T)$ is the recombination coefficient for the ion, and

$$\tau_\nu = N_X \int_r \sigma_\nu dr \tag{1}$$

is the frequency dependent optical depth. All these can be used to obtain an expressions for the photoionization rate,

$$I_X = \int_{\nu_X}^{\infty} \frac{(L_\nu/h\nu)\sigma_\nu e^{-\tau_\nu}}{4\pi r^2} d\nu \ , \tag{2}$$

and the recombination rate,

$$R_X = \alpha_X(T) N_e \ . \tag{3}$$

Thus, the ionization rate of ion X (cm^{-3} s^{-1}) is $N_X I_X$ and the recombination rate is $N_{X+1} R_X$.

We can now write a set of time dependent differential equations for the fractional ionization of all ions,

$$\frac{dN_X}{dt} = -N_X[I_X + R_{X-1}] + N_{X-1} I_{X-1} + N_{X+1} R_X \ , \tag{4}$$

where all other ionization and recombination processes have been neglected. The steady state solution for an element with n electrons and $n+1$ ions is a set of n equations of the type

$$\frac{N_{X+1}}{N_X} = \frac{I_X}{R_X} \ . \tag{5}$$

The additional relation needed for solving the set of equations is

$$\Sigma N_X = N_Z \ , \tag{6}$$

where N_Z is the total abundance of the element in question. This suggests that the level of ionization of the gas in photoionization equilibrium is proportional to I_X/R_X which, in turn (see Eqn. 2 and 3) is proportional to the photon number density divided by the electron density.

The above set of equations leads to the definition of two important time scales: the recombination time, $t_{rec} = 1/R_X$, and the ionization time, $t_{ion} = 1/I_X$. The first time scale gives the typical time required for ion $X+1$ to recombine to ion X, when the radiation source is turned off. The second time scale is the time required for X to get ionized to $X+1$ after a large increase in the ionizing flux. The recombination time depends on the particle (electron) density and the photoionization time depends on the photon number density. Thus, following a time dependent recombination process provides a way to probe the local conditions while following a time-dependent ionization enables to set a limit on the local radiation field, i.e. the distance from the source.

The simplest example of time dependent equations of this type are related to the ionization and recombination of hydrogen. In this case

$$\frac{dN_{H^0}}{dt} = -I_{H^0} N_{H^0} \ ; \ \frac{dN_{H^+}}{dt} = -\alpha(H) N_e N_{H^+} \tag{7}$$

with the trivial solutions

$$N_{H^0} = N_{H^0}(0) exp(-I_{H^0} t) \ ; \ N_{H^+} = N_{H^+}(0) exp(-\alpha(H) N_e t) \ . \tag{8}$$

For $T = 10^4$ K, $\alpha(H) \sim 10^{-13}\ cm^3 s^{-1}$. In this case

$$t_{rec} = \frac{1}{\alpha N_e} \simeq \frac{10^{13}}{N_e} \text{ sec.} \tag{9}$$

The recombination and ionization time scales can be quite different, depending on the radiation field and the gas density. Moreover, the coupling between

the various stages of ionization suggests that, under various conditions, the fractional abundance of ion X may change very slightly, or remains almost constant, despite large changes in the radiation field. Perhaps more important are the global recombination and ionization time scales which are the times required for the entire atmosphere to undergo a significant change in the level of ionization. Both are roughly given by $1/R_X$ where X is the *most abundant* ion of the element in question.

2.2 Additional ionization and recombination processes

While photoionization from the ground level, and radiative recombination following cascade, are the dominant processes in many cases of astrophysical interest, other processes must be considered too. The most important ones in AGN gas are:

Dielectronic recombination: This term refers to recombination through excited states. The process involves one free and one bound electrons that combine, for a short time, to form a highly excited state above the ionization threshold. The excited system can decay via "auto-ionization" (i.e. returning to its original state), or via recombination which result in a more neutral ion. Dielectronic recombinations is traditionally divided into "low temperature dielectronic recombination", due to $\Delta n = 0$ transitions, where n is the energy level in question, and "high temperature dielectronic recombination" involving $\Delta n = 1$ transitions. The first type is important for many elements at $T_e = 1 - 3 \times 10^4$ K and the second for hot ($T_e \sim 10^{6-7}$ K) plasmas.

Auger ionization: Ionization from inner shells due to absorption of high energy X-ray photons is important for ions with three or more electrons. The ejection of the inner electron results, in most cases, in the ejection of one or more electrons and even higher ionization. In a small fraction of the cases, the relaxation to the ground state involves the emission of a line photon, in most cases due to $2p-1s$ transitions. This fraction is called the "fluorescence yield" and is strongly dependent on the charge of the atom in question. For low ionization oxygen ions it is of order 0.01 and for iron ions it is typically 0.3.

Auger ionization couples non-adjacent stages of ionization and must be treated accordingly. For the most abundant elements with $Z < 26$, the inner shell ionization involves a doubly ionized atom (i.e. two stages above the ion that absorbs the high energy photon). For iron and heavier elements, more ionization are common, depending on the number of inner shell electrons.

Heating and ionization by secondary electrons: This process is important for gas with a very low level of ionization which is exposed to a large flux of high energy photons. The energetic electrons ejected due to the absorption

of such photons can collide with neutral atoms (mostly hydrogen) and cause additional ionization before they are thermalized. They can also collisionally excite $n > 1$ levels causing additional line emission.

Charge exchange: Charge exchange collisions between ions

$$X + Y^+ \rightleftharpoons X^+ + Y \tag{10}$$

can be very fast leading to a significant changes in the level of ionization under favorable conditions. An important example for photoionized gas at low temperatures involves neutral hydrogen and singly ionized oxygen. This reaction is known to be very fast under conditions prevailing near the hydrogen ionization front. Other important examples are the charge exchange of neutral nitrogen with ionized hydrogen and charge exchange of several ions with He^+.

Collisional ionization and three body recombination: These processes can be described as

$$X + e \rightleftharpoons X + e + e \ , \tag{11}$$

They are negligible for most ions for temperatures below $few \times 10^5$ K. Collisional ionization dominates the ionization of the gas in starburst regions and near shock fronts. In AGN, both processes can also become important in a high density, large optical depth gas where they can dominate the population of the high-n levels of hydrogen and helium.

Compton ionization, heating and cooling Photon-electron collisions can heat or cool the electron gas. In particular, the inverse Compton process can be a major source of cooling for a highly ionized gas.

2.3 Thermal balance

The thermal structure of the gas is determined by the balance between various heating and cooling processes that are noted here with H for heating and C for cooling, both in erg cm^{-3} s^{-1}. This is normally described by a set of equations that involves *energy* terms rather than *ionization and recombination* terms. The most important heating in AGN gas is due to photoionization (bound-free) which, for ion X, is given by

$$H_{bf,X} = N_X \int_{\nu_X}^{\infty} \frac{L_\nu \sigma_\nu e^{-\tau_\nu}}{4\pi r^2} d\nu \ . \tag{12}$$

Note that in this equation we sum over the absorbed energy while in the photoionization equation (Eq. 2) the sum is over the number of ionizing photons.

Similarly, an important cooling term is *recombination cooling* which, for ion X, is given by

$$C_{bf,X} = N_{X+1} N_e \alpha_X(T)[h\nu_{1,\infty} + h < \nu_{free} >] \tag{13}$$

where $h\nu_{1,\infty}$ is *the minimum* ionization energy from the ground level of the ion and $h < \nu_{free} >$ is the mean energy of a free recombining electron ($\sim kT_e$).

The above heating and cooling terms are simple manifestations of energy conservation. They are different from standard heating and cooling expressions given in other books where only *the energy of the free electrons* is considered. In that case, the term L_ν in the heating integral should be replaced by $(L_\nu/h\nu)(h\nu - h\nu_X)$ and the recombination cooling equation does not include cascade to the ground (the $h\nu_{1,\infty}$ term). The two treatment are exactly equivalent and all other heating and cooling terms can be computed with either approach provided they are used consistently.

Free-free is another cooling process. It is especially important in fully ionized plasma where it can be the dominant way of loosing energy by the gas. The rate for ion X with charge Z is,

$$C_{ff,X} = 1.42 \times 10^{-27} Z^2 T^{1/2} g_{ff} N_e N_{X^{+z}} \ . \tag{14}$$

Many cases of astrophysical interest includes gas which is not fully ionized. In general, the most important cooling term in such cases is line cooling due to bound-bound (bb) transitions. The computation of this term, denoted C_{bb}, requires a complete solution of the level population for all ions of importance.

The most important contributers to the level populations in AGN gas are recombination and cascade, emission and absorption of line photons, and collisional excitation and de-excitation of bound states. Consider first bound-bound transitions between levels i and j, where $j > i$, that result, eventually, in bb cooling. The collisional excitation rate between the levels is

$$q_{ij} = C_{ij} N_e \ , \tag{15}$$

where

$$C_{ij} = \frac{8.63 \times 10^{-6}}{\sqrt{T}} \frac{\Omega_{ij}}{\omega_i} e^{-E_{ij}/kT} \ . \tag{16}$$

Likewise, the collisional rate from j to i is

$$q_{ji} = C_{ji} N_e \ , \tag{17}$$

where

$$C_{ji} = C_{ij}\frac{\omega_i}{\omega_j}e^{E_{ij}/kT} \ . \tag{18}$$

Here w_i and w_j denote the statistical weights of levels i and j and Ω_{ij} is the effective collision strength that is obtained from quantum-mechanical calculations. The calculation of C_{bb} requires, therefore, a complete knowledge of all level populations at all times.

Solving for the level populations involves a large set of time dependent statistical equilibrium equations. To illustrate this we consider a simple two-level system and only three processes: recombination with a rate $\alpha_{eff,2}$, collisional excitation and de-excitation with rates q_{12} and q_{21} respectively, and line (but no continuum) photon emission and absorption. Consider first a case of very small optical depth in the $2-1$ transition. The time dependent equations can be written as

$$\frac{dn_2}{dt} = n_1 q_{12} - n_2(A_{21} + q_{21}) + N_{X+1}N_e\alpha_{eff,2} \tag{19}$$

with the additional constraint

$$n_1 + n_2 = N_X \ . \tag{20}$$

The level population are time dependent since the ionic abundance and the electron temperature are time dependent. The solution of the two equations results in the level population of n_1 and n_2 at all times. Additional processes that have been neglected so far, and were mentioned earlier as potentially important, are dielectronic recombination, collisional ionization of both levels, three body recombination, photoionization from both levels and continuum pumping that will be explained later. Most of these can easily be added to the above equations.

Having solved for n_1 and n_2, we can now express the line emissivity, ϵ_{21}, as

$$\epsilon_{21} = n_2 A_{21} h\nu_{21} \, . \tag{21}$$

where ϵ_{21} is time dependent too. The bb cooling term associated with such processes is the sum over all lines,

$$C_{bb} = \Sigma_{j>i}\epsilon_{ji} \ . \tag{22}$$

The expression for C_{bb} contains the hidden assumption that the emitted radiation in all lines can *freely escape the medium*. In such a case, a photon emitted

in a certain location carries with it the maximum possible energy, $h\nu_{21}$, which results in maximum cooling. However, this assumption is not always true. Some lines, in particular the leading resonance lines of hydrogen, helium and the more abundant metals, can become optically thick to their own radiation. A line photon emitted in such a transition can be absorbed in a different location in the gas contributing additional heating at that point and increasing the n_2 level population there. For lines with large optical depth, the absorbing location is close to the location of emission. For lines of small optical depth, this can be in a different part of the cloud.

A simple, not very accurate way to deal with this complication is to introduce the "line escape probability" which gives the probability of line photons to leave the point where they are created without being absorbed by another 1–2 transition. This escape probability, which is indicated here with β_{12}, can be specify as an average property, over the entire cloud (a "mean escape probability") or as a local quantity (a "local escape probability"). All that is required is to replace A_{21} in eqn. 21 by $\beta_{21}A_{21}$, i.e. not to count those photons absorbed on the way out. Thus the local n_2 level population is increased by a factor of $1/\beta_{12}$ relative to the previous case and the line emission is replaced by

$$\epsilon_{21} = n_2\beta_{21}A_{21}h\nu_{21}\,. \tag{23}$$

The net result for a two level system, in the absence of non-radiative processes, in no change in local cooling, or in emergent line emission, relative to the case of $\beta_{12} = 1$. In reality this is not the case since transitions to and from other levels must be included, collisional suppression of the upper level can become important, etc.

The above treatment replaces the more rigorous, full radiative transfer solution. It enables a full local solution but neglects radiative coupling of different locations in the gas. Detailed radiative calculations show that a reasonable approximation is $\beta_{12} = 1/(1 + b\tau_{12})$, where τ_{12} is the optical depth between the two levels and b is a constant of order unity. Extensive theoretical studies show that the escape probability formalism, in which each line is assigned it own escape probability, is an adequate method to deal with many resonance transitions. The approximation is more problematic when dealing with the hydrogen atom since, in such cases, the strong AGN radiation filed can result in clouds of large column density where hydrogen is almost fully ionized. In such cases, the hydrogen level 2 population can be large and the optical depth in the Balmer lines significant. This, couples with the extremely large optical depth of the Lyman lines, makes line transfer and photon diffusion in the cloud more difficult to treat and reduces the usefulness of the escape probability approach.

Having computed the individual heating and cooling processes, we can now write the general energy equation,

$$H = C \ , \tag{24}$$

where

$$H = \Sigma_i H_i \tag{25}$$

and

$$C = \Sigma_i C_i \tag{26}$$

are sums over all heating and cooling terms. The solution of this equation is used to obtain the kinetic temperature of the gas. This is relatively simple in steady state, where the level population and ionization fractions are not time dependent. The main complications are due to radiative transfer in optically thick line and continua that couple the level populations to the gas temperature through collisional excitation and de-excitation processes.

2.3.1 Mechanical heating of AGN gas

The temperature and ionization of AGN gas are controlled, primarily, by the central radiation field. This is in contrast to different environments, such as star-forming regions, where mechanical heating is the dominant heating source and most ionization is due to collisional processes. Such AGN gas can indeed be affected by collisional processes. For example, small-scale jets can transfer a large amount of mechanical energy into a very small region, producing strong shocks and bright emission knots typical of collisionally excited plasma. However, general considerations suggests that such processes cannot be globally important in the type of environment considered here.

Consider the mechanical energy produced by a shock of velocity v_{sh}. This is given roughly by $\frac{1}{2} m_{sh} v_{sh}^2$ where m_{sh} is the mass of the flowing material. We can assign an efficiency factor, η_{sh}, to this process which, in units of mc^2, is $\frac{1}{2} v_{sh}^2 / c^2$. Equivalently, if m_{acc} is the mass of the gas accreted by the BH then the energy associated with this process is about $\eta_{acc} m_{acc} c^2$, where η_{acc} is the mass to energy conversion factor in the accretion process. The velocity of the bulk of the line emitting gas in AGN is 500–1000 km s^{-1} and for accretion disks around massive BHs, $\eta_{acc} \sim 0.1$. The ratio of the energies produced by the two processes is approximately

$$\frac{\eta_{acc} m_{acc}}{\eta_{sh} m_{sh}} \simeq 10^5 \frac{m_{acc}}{m_{sh}} \ . \tag{27}$$

Thus, for shock excitation to be energetically significant, the amount of flowing shocked gas must exceed, by many orders of magnitude, the amount of material accreted onto the BH.

2.4 The spectrum of ionized AGN gas

2.4.1 Ionization parameter

The earlier discussion suggests that the level of ionization of photoionized gas depends on I_X/R_X (eqn. 5) which is proportional to the ratio of the ionizing photon density over the gas density. Given the conditions of photoionization equilibrium, one can define an "ionization parameter" which is proportional to this ratio. A possible definitions is

$$U = \int_{E_1}^{E_2} \frac{(L_E/E)dE}{4\pi r^2 c N_{\rm H}} \ , \tag{28}$$

where c, the speed of light, is introduced to make U dimensionless and E_1 and E_2 are the energies defining the limits of integration over the ionizing continuum. The value of U defined in this way gives a good indication for the level of ionization provided E_1 is close to the minimum energy require to ionized the most "important" (cooling-wise) ions. For gas that is ionized by soft-UV radiation, E_1 should be chosen such that it is related to the UV ionizing field, e.g. the energy of the hydrogen Lyman limit at 13.6 eV. An appropriate name in this case is U(hydrogen). Similarly, a suitable choice for gas whose level of ionization is dominated by a strong soft X-ray source is $E_1 = 0.1$ keV and $E_2 = 10$ keV. This is usually assigned the symbol $U(X-ray)$ or U_X. Such gas can be transparent to UV photons and U(hydrogen) is not a good indicator of its level of ionization. An alternative suitable choice for the case of X-ray dominated gas might be $E_1 = 0.54$ keV, corresponding to the K-shell threshold ionization of oxygen, the most important emitting and absorbing element under such conditions. A suitable name is U(oxygen). There are other, somewhat different definitions of the ionization parameter that are used in the literature. A common one, ξ, is defined by the energy flux, rather than the photon flux, and is given by

$$\xi = \int_{13.6\ \rm eV}^{13.6\ \rm keV} \frac{L_E}{r^2 N_H} dE \ . \tag{29}$$

Using the "right" ionization parameter, we normally find that $U = 10^{-1} - 10^{-2}$ corresponds to gas that produces strong emission lines in the energy range

Table 1
Various ionization parameters used in AGN research

Ionization parameter	E_1	E_2	conversion factors, $L_E \propto E^{-1.3}$
U(hydrogen)	13.6 eV	∞	1000
U(helium)	54.4 eV	∞	165
$U(\mathrm{X-ray})$	0.1 keV	10 keV	73.3
U(oxygen)	0.54 keV	10 keV	8.2
ξ	13.6 eV	13.6 keV	31.1

under question. For example, $U(\text{oxygen}) = 0.1$ results in strong 0.5-3 keV emission lines. A much smaller U results in more neutral gas, with very little X-ray emission, and a much larger U results in very highly ionized gas and insignificant line emission. Table 2.4.1 gives a list of several ionization parameters that are useful in various situations and are commonly used in AGN research. The right column of the table allows a simple conversion between those ionization parameters for the case of $L_E \propto E^{-1.3}$.

2.4.2 Line and continuum emitting processes

The most important continuum emitting processes in AGN gas are due to bound-free transitions. The clear signature of such processes in the optical-UV band are the bound-free edges of levels $n = 1$ and $n = 2$ of hydrogen and helium. In the X-ray band the observationally important processes are bound-free transitions to the ground levels of H-like and He-like carbon, nitrogen, oxygen, neon, magnesium and silicon. Free-free emission is important at radio frequencies, in a low temperature gas, and at hard X-ray energies in a high temperature plasma.

Line emission (bound-bound) transitions dominate the heating-cooling balance in low ionization ($U(\text{hydrogen}) \sim 0.01$) photoionized gas. The most intense transitions are due to forbidden lines, in low density gas, and due to recombination and collisionally ionized permitted lines, in high density gas. For highly ionized X-ray gas ($U(\text{oxygen}) \sim 0.01$), most cooling is via bound-free transitions because the lowest accessible levels are at energies that are much larger than kT. This gas is dominated by permitted, intercombination and forbidden recombination lines. Starburst heated X-ray gas, which is sometimes found in AGN, is characterized by higher temperatures and lower densities. The most intense lines in such gas are produced via collisional excitation of the $n = 2$ and $n = 3$ levels of the more abundant elements.

There are several additional line and continuum emitting processes that become important under favorable conditions. Two of those are:

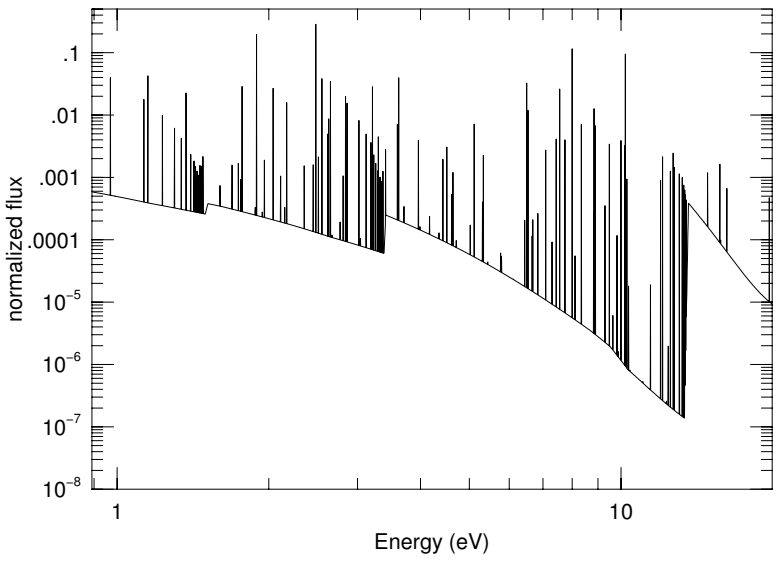

Fig. 4. The spectrum of optically thin $T_e \sim 10^4\,\mathrm{K}$ $N_H \sim 10^6$ cm^{-3} photoionized gas, showing the strong bound-free recombination edges (in this case, the Lyman, Balmer and Paschen jumps) and many emission lines.

Continuum fluorescence: This process, sometimes referred to as "photoexcitation" or "continuum pumping", is the result of populating low lying levels by absorbing the incident continuum in various resonance transitions. This increase the level population and results in additional line emission. The effect on the global energy balance is negligible, especially in low density environment, since most of the radiation can escape the gas. Thus, heating and cooling almost exactly balance.

The increase or decrease in the observed line intensity, due to this process, is geometry dependent. For example, in a static spherical atmosphere, or in a static spherical thin shell around a point continuum source, the process can be considered as pure scattering since emission is exactly balanced by absorption. In a moving spherical atmosphere, the emitted photons are Doppler shifted relative to the gas rest frame, and absorption and emission appear at different energies. This results in a P-Cygni line profile with the same equivalent widths (EWs) for emission and absorption. In cases of incomplete covering, like a broken spherical shell, absorption is stronger than emission in terms of the measured EW, provided the line of sight passes through the absorber. Finally, for optically thick lines, the absorption and emission optical depths are geometry (e.g. direction) dependent and are not necessarily the same. This can affect the emergent line intensity.

Continuum fluorescence in the X-ray band can also excite inner shell transitions. In principle, this is similar to absorption by resonance lines except that some of these transitions can result in an autoionized stage above

the threshold ionization energy of the valence electrons. This can result in either ionization or recombination depending on the level in question. Autoionization dominated transitions result in almost no line emission. Such transitions can be seen as X-ray absorption lines and the process can affect the ionization and heating of the gas.

Line fluorescence: As explained earlier, the ejection of inner shell electrons can lead to line emission ("fluorescence lines"). The process is important at X-ray energies where lines of this type, most notably iron Kα and Kβ lines, in the 6.4–9.0 keV energy range, are occasionally observed. The fluorescence efficiency ("fluorescence yield") depends on Z^3 and is roughly 0.3 for iron. Thus, the most abundant elements, like oxygen, do not produce strong fluorescence lines, despite the order of magnitude difference in abundance between iron and oxygen. This difference can partly be compensated for by the larger incident flux around 0.54 keV (the K-shell threshold for neutral oxygen), compared with the flux near 7.1 keV (the K-shell threshold of neutral iron).

2.5 Gas composition

There are several standard ways to measure the composition of ionized plasma. The most accurate methods are based on the comparison of the intensities of metal recombination lines, with known effective recombination coefficients, with Hα or Hβ. Such methods depend on the ability to measure the recombination lines that are typically very weak and often undetected. A less accurate but more practical method is based on the comparison of the intensities of various collisionally excited lines. Unfortunately, these methods that were developed for low density gas, e.g. in planetary nebulae and HII regions, fail to give reliable answers in AGN, especially in regions of very high density like the BLR. There are two reasons for the failure, one is the high density where many levels are collisionally suppressed by unknown amounts and the other due to complication in calculating, accurately, the intensities of optically thick lines like Lyα and Hβ.

Several methods have been developed in order to circumvent these difficulties. In particular, the N V λ1240/C IV λ1549 line ratio (hereafter the NV/CIV method) has been suggested as a good N/C abundance indicator in BLR gas. These lines are easy to measure either with space-borne spectrographs, in low redshift sources, or from the ground, in high redshift AGN. The idea is that the abundances of all α elements (C, O, Mg etc.) relative to hydrogen are increasing together and represent the star-forming rate. Thus C/H, O/H etc. are all proportional to the metallicity (Z) of the gas. Nitrogen is a secondary element and we expect that for large enough metallicity ($Z \geq 0.2$) $N/H \propto Z^2$. Given these relations, we expect that NV/CIV$\propto Z$.

The crucial question is under what condition is the N v λ1240/C iv λ1549 line ratio a good N/C abundance indicator. This is related to the rather different level of ionization of C^{+2} and N^{+3} and the somewhat different excitation energies. This question has been investigated, theoretically, by computing numerous photoionization models with various assumptions about the ionization parameter, gas density and SEDs. In most those calculations there is, indeed, a good correlation between the actual N/C abundance ratio and the value obtained from the N v λ1240/C iv λ1549 line ratio.

A more promising method is to search for line ratios that are insensitive to ionization and local temperature conditions, i.e. lines from ions with overlapping production regions and similar excitation energies (to eliminate the strong dependence on temperature through the the $\exp(-E_{ij}/kT)$ factor). Some examples of such line pairs are O iii]λ1663/C iii] λ1909 that can be a good O/C indicators and N iv]λ1486/C iv λ1549 which is a good N/C indicator. This method, which is probably best, is difficult to apply since most of the lines in question are weak and difficult to measure. Moreover, several of the lines are semi-forbidden lines with critical densities that are close to the typical density of the BLR gas. Thus, there are uncertainties due to the unknown gas density which affect the observed line intensities.

The general results of such studies is a large metallicity range, $1 \leq Z \leq 5$, with several examples of $Z > 10$. There are several interesting suggestions that connect the high measured metallicity to other properties of AGN. One is that the gas metallicity (more specifically the NV/CIV line ratio) depends on the source luminosity. Other possibilities are a dependence on the black hole mass and/or the accretion rate. At this stage there are not enough measurements of objects with well determined mass and accretion rate estimates to decide between all those.

2.6 Clouds, condensations, confinement and winds

The basic line emitting entity in AGN is normally referred to as a *cloud*. The assumption of clouds, or more generally condensations, is reasonable given the observations of galactic HII regions, and the interstellar medium, where condensations are indeed observed. Clouds are also required by line intensity considerations, mainly the observation that the typical observed line widths, e.g. in the BLR, are similar for low and high ionization lines. A configuration in which every ionization stage is associated with a certain location and thus a certain velocity cannot explain the observed line profiles. On the other hand, an ensemble of small clouds, each optically thick and each producing many emission lines with a large range of ionization, is more plausible. This however is somewhat problematic since such entities must be either gravitationally

bound or else confined by external pressure.

Likely candidates for self gravitating clouds are stars in the central cluster. In particular winds produced by "bloated stars" have been considered as the origin of material in the broad and the narrow line regions. It it interesting to note that "typical" NLR clouds (that are not just theoretical entities since direct observations of nearby AGN show clear condensations in the NLR) contain masses of about one $M_\odot$. Much lower mass clouds, containing as little as 10^{-8} $M_\odot$, have been considered in various BLR models. Such clouds must be confined or else be created and destroyed on a sound speed crossing time, which is very short. For the BLR clouds, this time is of order one year.

The most likely confinement mechanisms for clouds that are not self-gravitating are either thermal confinement, by a low density hot inter-cloud medium (HIM), or confinement by magnetic fields. The conditions for pressure equilibrium are obtained from general considerations of a two-phase medium, similarly to what is done in the ISM.

Consider a medium where the fractional ionization of the gas and its kinetic temperature are determined solely by the central radiation field. Suppose there are two components at the same location with different temperatures, densities and levels of ionization, that are noted 'cold" and "hot". In this case,

$$U_{cold} \propto \frac{L/c}{r^2 N_H(cold)} \ ; \ U_{hot} \propto \frac{L/c}{r^2 N_H(hot)} \ . \tag{30}$$

At a given distance r, the radiation pressure is simply $P_{rad} \propto L/cr^2$ and is independent of the gas density. This means that $U \propto P_{rad}/N_H$. Dividing U by the relevant temperature (T_{cold} or T_{hot}) and noting that all quantities are calculated at the same location, we find that the condition for pressure equilibrium due to the same gas pressure in the two compensate leads to

$$\frac{U_{cold}}{T_{cold}} = \frac{U_{hot}}{T_{hot}} \propto \frac{P_{rad}}{P_g} \ . \tag{31}$$

Thus, for all components at the same chosen location $U/T \propto P_g^{-1} \propto (N_H T)^{-1}$. This allows several different temperatures, and hence several values of the density, at the same location provided U/T is the same for all components. Such two (or more) components can survive, side by side, in pressure equilibrium, provided they are stable against thermal perturbations. The situation is illustrated in Fig. 5 that shows the famous "S-curve", which is the photoionization equilibrium curve (sometimes referred to as the "stability curve") for such gas. Each point on the curve is characterized by thermal equilibrium ($H = C$) at a different temperature. The points outside the curve are regions where either $H > C$ (on the right hand side of the stability curve) or in the region where

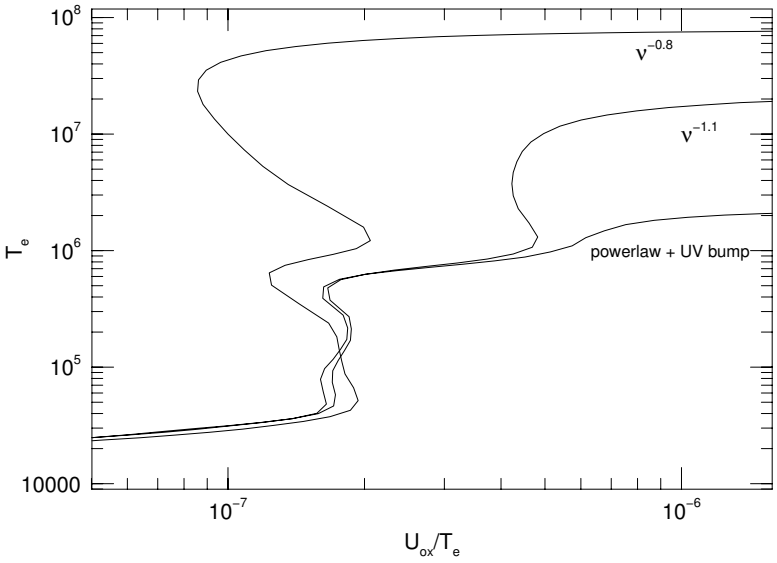

Fig. 5. Stability curves for different SEDs: 1. $L_E \propto E^{-0.8}$. 2. $L_E \propto E^{-1.1}$. 3. "Typical" AGN SED with a strong blue-bump and an X-ray power-law. Note the several unstable regions (negative slope parts) that are less noticeable in the SED containing a UV bump. Such a SED results in lower T_C due to the efficient Compton cooling by the blue-bump radiation.

$H < C$ (on the left hand side of the curve). These represent pairs of U and T which cannot be found in gas of the same composition which is in thermal equilibrium.

The upper branches of the stability curves shown here are stable, i.e. a small deviation from the curves results in return to an adjacent stable region. Their temperature is close to the Compton temperature of the fully ionized gas which is determined solely by Compton heating and cooling and is given by,

$$T_C = \frac{h\overline{\nu}}{4k}\,, \tag{32}$$

where $h\overline{\nu}$ is the mean photon energy weighted by the cross section. T_C depends only on the SED and, for AGN, is $\sim 10^7$ K. The lower branch with the positive slope is also stable and is typical of AGN photoionized gas with a characteristic temperature of $\sim 10^4$ K. For example, an increase in the incident flux results in increasing U. On the positive slope part of the stability curve, this will result in an increase of T which will take the gas to an adjacent equilibrium point just above the starting point.

The intermediate part contains one or more regions with negative slopes. These

are unstable regions where small perturbations to the right (the region where $H > C$) due to additional heating, or to the left ($H < C$) due to reduced heating. This will result in further removal from the stability curve. There is no nearby solution and the gas can reach thermal equilibrium only in a place with very different values of U and T. This is the clear signature of an unstable gas. The curve shown suggests that there are values of U/T that correspond to two and even three stable (positive slope) solutions. Thus a two or three-component medium can be formed in gas exposed to a typical AGN radiation field. Such localized components, with well defined temperatures and densities, could be described as "clouds" or condensations.

An alternative and perhaps a more likely situation is confinement by magnetic pressure. In this case, $B^2/8\pi \geq (N_H + N_e)kT$ and the required magnetic field is of the order of one gauss for the BLR and much smaller for the NLR. The "clouds" in this case are likely to have a non spherical shape, perhaps elongated filaments along the magnetic field lines.

Another alternative to the pressure confined clouds are condensations or filaments that are constantly produced and destroyed. Such situations are common in the interstellar medium and have also been considered for AGN. One model that attracted much attention is the locally optimally emitting cloud (LOC) model which involves an assumed range of density, column density and covering factor at any given location. The various components in this model are not in pressure equilibrium and little is known about their formation and stability. The calculated spectral properties are quite appealing since they produce a good fit to the observed optical-UV spectrum of many AGN. Here, again, there are several ad-hoc assumptions that must be made in order to specify the various properties of such medium.

Finally we consider gas outflow from the central disk, or from other large mass reservoirs, in the form of a continuous wind. Such flows are characterized by continuous change of density and velocity and are very different from the above considered "clouds". The emission and absorption spectrum of such flows are very different from those produced by clouds mostly because of the different opacity distribution and the location of the various ionization fronts.

2.7 Photoionization models

Putting all the above together is not a simple task. It is normally achieved with the help of photoionization models that include the calculations of all the processes mentioned above and more. A given model solves, numerically, for the ionization and thermal structure within *one cloud*. Most present day models are time independent since time-dependent processes are more difficult

to treat. The transfer of radiation is done, in most cases, with an escape probability formalism but more sophisticated methods have been tried too.

Having calculated the ionization and thermal structure, and the steady state level population of all abundant ions, one can now use these properties to calculate a theoretical emission line spectrum which will then be compared with observations. Such calculations involve some assumptions about the cloud distribution in space and their other properties such as density, column density and shape. A simple approach is to assume a line emitting region which is made of numerous small clouds whose density, dimension and other properties depend solely on the distance r. Confinement is achieved by hot gas (HIM), by magnetic pressure, or perhaps by something else. The exact mechanism is not important provided the pressure of the confining medium/agent is a simple function of the radius, $P \propto r^{-s}$. The contribution of each cloud to the various emission lines is determined by the physical conditions within the cloud and its distance from the center. We can also assume a spherical geometry around the central radiation source and simple radial dependence of all cloud properties.

Having defined the external pressure, we find that the hydrogen number density, $N(r)$ is controlled by the equilibrium with the external pressure. Neglecting the small electron temperature variation inside the cloud we can take this to be identical to the external pressure distribution, i.e.,

$$N_H(r) \propto r^{-s} \quad . \tag{33}$$

Next, we define the cloud column density, N_{col}, by considering spherical clouds of radius $R_c(r)$. The mass of the individual clouds is conserved, as they move in or out, but it is not necessarily the same for all clouds, thus, $R_c^3(r)N(r) = const.$ The cloud mean (over the sphere) column density is thus

$$N_{col}(r) \propto R_c(r)N(r) \propto r^{-2/3s} \quad , \tag{34}$$

and the geometrical cross-section is

$$A_c(r) \propto R_c^2(r) \propto r^{2/3s} \quad . \tag{35}$$

Finally, the number of clouds per unit volume is

$$n_c(r) \propto r^{-p} \ , \tag{36}$$

where p is an additional parameter which is required to fully define the calculation.

The next step requires the integration over the entire system. This is simplified by assuming only one type of clouds. Simple generalization of this scheme can involve a local population of clouds having some size distribution.

The clouds in question are illuminated by a central source whose ionizing luminosity, $L(t)$, varies in time. Designating $\epsilon_l(r, L)$ as the flux emitted by the cloud in a certain emission-line, l, per unit projected surface area ($erg\ s^{-1}\ cm^{-2}$), we get the following relation for the emission of a single cloud:

$$j_{c,l}(r, L) = A_c(r)\epsilon_l(r, L) \quad . \tag{37}$$

Assuming the clouds extends from r_{in} to r_{out} we obtain the cumulative line fluxes,

$$L_l \propto \int_{r_{in}}^{r_{out}} n_c(r) j_{c,l}(r, L) r^2 dr \quad . \tag{38}$$

Having determined the properties of the emission line clouds, we now calculate $\epsilon_l(r, L)$ using a photoionization code. We then follow the above formalism to obtain E_l. Since all parameters have been fixed, there is no need to independently specify the ionization parameter, $U(r)$ which, in this model, is given by

$$U(r) \propto r^{s-2} \ . \tag{39}$$

A complete model of this type, with a given gas composition, is specified by the source luminosity and SED, the radial parameter s, the boundaries r_{in} and r_{out}, and the normalization of the density and column density at a fiducial distance. The comparison with the observations further requires the normalization of the total line fluxes. This is better defined by using the total covering factor, $C_f(r_{out})$, which is obtained by integrating

$$dC_f(r) = A_c(r) n_c(r) dr \propto r^{2/3s-p} dr \tag{40}$$

between r_{in} and r_{out}. The normalization of $C_f(r_{out})$ is achieved by comparing the observed and calculated flux of the emission lines. In all this we did not consider cloud obscuration and the possibility that radiation emitted by one cloud is absorbed by another. Thus, such models are limited to $C_f(r_{out})$ smaller than about 0.3.

As noted earlier, there are alternatives to the small clouds model. In particular, the LOC model assumes numerous clouds, with a range of properties like density, column density and covering fraction, at any given location. The main

suggestion is that the local ionizing flux, and the gas density, produce a large range of ionization parameter at any given locations. Lines from high and low ionization species are produced, with different efficiencies, at all radii, and the local spectrum reflects the range of physical properties. The $1/r^2$ flux variation across the system is the main reason for the different contributions to the various emission lines at different locations.

2.8 Collisionally ionized plasma

While most of the gas in AGN is photoionized by the intense radiation field, some regions, in particular those associated with star formation, may be heated and ionized by shock due to fast stellar winds and super-novae explosions. The resulting collisional ionized plasma can be very different in its thermal and ionization properties from photoionized gas. Its emitted spectrum will carry the signature of the dominant line and continuum producing processes and its analysis can reveal some of those properties. In general, the micro-physics in such regions is dominated by collisional processes and typical temperatures can be orders of magnitude larger than those observed in photoionized gas with a similar level of ionization. Different tools are needed to analyze such gas.

2.9 The motion of ionized gas

2.9.1 The equation of motion

AGN gas is exposed to a strong radiation field that can, under certain conditions, produce large-scale flows. Such flows can be continuous, in which case they are classified as "winds", or else drive clouds or condensations in a ballistic way (the general term "wind" as used in the literature can include condensations inside a continuous flow).

The general form of the equation of motion for a cloud of mass M_c is

$$a(r) = a_{rad}(r) - g(r) - \frac{1}{\rho}\frac{dP}{dr} + f_d/M_c \ , \tag{41}$$

where $g(r)$ is the gravitational acceleration, $a_{rad}(r)$ the acceleration due to radiation pressure force and f_d the drag force. For pure wind flows we neglect the drag force term and the internal radiation pressure. This gives

$$v\frac{dv}{dr} = a_{rad}(r) - g(r) - \frac{1}{\rho}\frac{dP_g}{dr} \ . \tag{42}$$

We also need an equation that describes the location dependent density of the flow. This is obtained from the continuity condition

$$\dot{M} = 4\pi\rho r^2 v C_f(r) = const. \ , \tag{43}$$

where $C_f(r)$ is the location dependent covering factor of the outflowing gas. For ballistic flows $\dot{M}$ needs to be specified more carefully, given the initial conditions, the number of moving clouds and the flow geometry.

The relative importance of the various terms in the equation of motion depend on the local conditions. Gravity dominates in almost all cases of low ionization, large column density gas. The reason is that the neutral gas at the part of the cloud away from the illuminated surface is not affected by the radiation pressure force. Radiation pressure force dominates the motion of ionized, low optical depth gas near a source with a high accretion rate and large η. This is not the case for fully ionized gas where only electron scattering contributes to the pressure. Pressure gradient can be the dominant factor when $a_{rad}(r) \ll g(r)$ and when the volume is filled with high ionization, high temperature gas.

2.9.2 Radiation pressure

The equation required for calculating the radiation pressure force at a distance r is obtained by summing over all absorption processes. In this equation the contribution to a_{rad} due to ion X is

$$a_{rad}(r, X) = \frac{N_X}{\rho(r)c} \int_{\nu_X}^{\infty} \frac{L_\nu \kappa_\nu e^{-\tau_\nu} d\nu}{4\pi r^2} \ . \tag{44}$$

The term κ_ν, gives the total absorption cross section per gram, including all bound-bound, bound-free, free-free and Compton scattering processes. It is different from the photoionization cross section, σ_ν, used in Eqn. 2, which is the bound-free cross section per particle.

The relationship between a_{rad} and the level of ionization can be understood by considering the important case where the largest contribution to the radiation pressure force is due to ionization (i.e. bound-free transitions). To illustrate this we assume that the mean energy of an ionizing photon is $\overline{h\nu}$ and use the definition of I_X from Eqn. 2. For ionized gas with $N_e \simeq N_H$ this gives

$$a_{rad}(X) \propto \frac{\overline{h\nu}}{cN_e} N_X I_X \ . \tag{45}$$

In a steady state case, photoionization is exactly balanced by radiative recombination which gives

$$N_X I_X = R_X N_{X+1} = \alpha N_e N_{X+1} \propto N_e^2 \ . \tag{46}$$

Thus a_{rad} is proportional to N_{X+1} and for the specific case of hydrogen,

$$a_{rad} \propto N_e \ . \tag{47}$$

It is customary to introduce the "force multiplier", $M(r)$, which is the ratio of the total radiation pressure to the Compton radiation pressure,

$$M(r) = \frac{a_{rad}(total, r)}{a_{rad}(Compton, r)} \ , \tag{48}$$

where

$$a_{rad}(Compton, r) = \frac{N_e(r)\sigma_T L}{4\pi r^2 \rho(r) c} \, . \tag{49}$$

$M(r)$ provides a convenient way of expressing the radiation pressure force in the equation of motion. Note that by definition $M(r) \geq 1$ and that $M(r) = 1$ for fully ionized gas.

For partly neutral gas, the main contributions to $M(r)$ are from bound-bound and bound-free transitions. The former dominates in those cases where the line optical depths are small. The contribution is much reduced for optically thick lines except for the illuminated surface of the gas. The Compton and free-free terms are usually small except for fully ionized plasma. Fig. 6 shows several examples of the various contributions to the force multiplier in a highly ionized AGN gas.

The gravitational and radiation pressure forces can be directly compared by writing the equation of motion in a slightly different form. This is done by noting that the mass of the central BH is proportional to L_{Edd} and the radiation pressure force is proportional to L. Denoting $\Gamma = L/L_{Edd}$ and noting that $L_{Edd} \propto M_{BH}$, we obtain

$$v\frac{dv}{dr} \simeq \frac{\sigma_T L}{m_H c 4\pi r^2}[M(r) - 1/\Gamma] - \frac{1}{\rho}\frac{dP_g}{dr} \tag{50}$$

for the wind equation of motion. The term $M(r) - 1/\Gamma$ in this equation gives the relative importance of gravity and radiation pressure. Thus sources of large Γ require smaller force multipliers to drive the wind. E.g. a source with

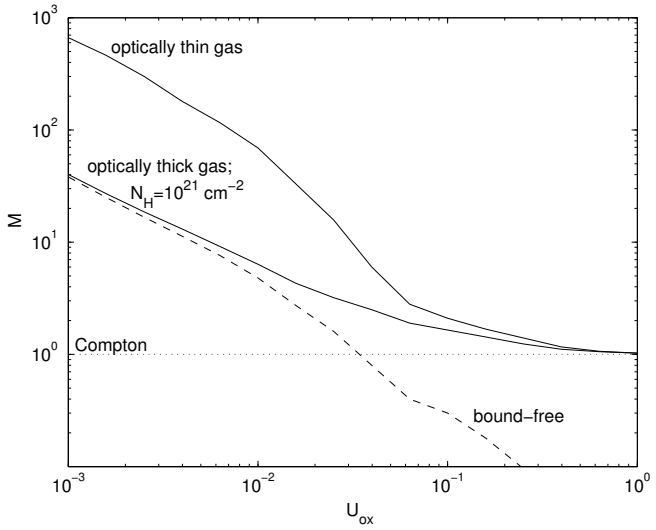

Fig. 6. The force multiplier calculated for a "standard AGN SED" and solar metallicity over a large range of the ionization parameter U(oxygen). The optically thin case includes free-free, bound-free and bound-bound contribution to M. Bound-bound absorption dominates for all levels of ionization except for almost completely ionized gas at large values of U(oxygen) . The large column density case is dominated by bound-free absorption since the resonance lines are very optically thick and do not contribute much to M (courtesy of D. Chelouche).

$\Gamma = 0.1$, typical of low and intermediate luminosity AGN, require $M \geq 10$ in order to drive a wind by radiation pressure force. Such large values of $M(r)$ are normally achieved only in situations where bound-bound transitions are important (see Fig. 6). Note that the constant multiplying $M(r) - 1/\Gamma$ in Eq. 50 is defined to within a factor of ~ 1.2 since the force multiplier and the Eddington ratio differ by the value of μ, the mean molecular weight per electron (this is the reason for the use of the $\simeq$ sign in Eq. 50).

AGN outflows are clearly recognized by their UV and X-ray absorption lines. The first indicate a large velocity range, from $few \times 10^2$ to $few \times 10^4$ km s^{-1}, while the latter are characterized by $v_\infty = few \times 10^2$ km s^{-1}. This can be translated to conditions near the base of the flow. As explained, the maximum velocity of AGN flows that are driven by bound-free dominated radiation pressure force is of the same order as the escape velocity at the base of the flow. The highest velocity, UV absorbing gas must therefore originate in the vicinity of the central BH and accretion disk. The slower X-ray outflows can originate much further out, perhaps outside the BLR. As explained, bound-bound radiation dominated flows can reach higher velocities.

3 Main components of AGN

The AGN phenomenon which is normally recognized by the association with the nuclear region of the host galaxy, can, in fact, cover a large range of radii and different physical conditions. The observed properties of AGN gas depend on its location, density, column density and composition. These determine the ionization parameter, the relative importance of radiation pressure force and the gas velocity. Other important factors are the local pressure (e.g. confinement) and the interaction with the other nuclear components. In the following we consider several possible locations, and gas properties, and discuss their observational signature.

3.1 The broad line region

Consider large column density ($\sim 10^{23}$ cm^{-2}) high density ($\sim 10^{10}$ cm^{-3}) gas clouds situated at a location where $L/4\pi r^2 \simeq 10^9$ erg s^{-1} cm^{-2}, i.e. about 1 pc for a very luminous AGN. Consider also that the clouds can survive over many dynamical times ($t_{dyn} \sim 300$ years in that location) An important consequence is that the cloud system is bound, because gravity dominates over radiation pressure force which is inefficient in such large column density material. The clouds typical velocity at this location is ~ 3000 km s^{-1} which will be reflected in the widths of the emitted line profiles. Finally, we assume a global (4π) covering factor of order 0.1. This means that we can neglect the absorption of the radiation emitted by the clouds on its way out.

The physical conditions assumed for this region result in U(hydrogen) $\sim 10^{-2}$. This means that only the illuminated surfaces of the clouds are highly ionized. The most abundant ions in the ionized parts are He III, O IV-VI, C III-IV, etc. The strongest emission lines are, therefore, Lyα, C IV λ1549 and O VI λ1035. The density is high but not too high to suppress all semi-forbidden lines. Strong predicted lines of this type are C III] λ1909 and O III] λ1663. Much of these large column density clouds must be partly neutral since only X-ray photons can penetrate beyond an hydrogen column of $\sim 10^{22}$cm^{-2}. These parts will produce strong lines of H I, Mg II and Fe II. The observed EWs of the strongest lines depend on the emissivity and covering factor. For the specified conditions assumed here they are of order 10–100 Å for the strong emission lines. Absorption lines are predicted to be extremely weak because of the small covering factor. A region with those observed properties and spectrum would justify the name "broad line region" (BLR).

Can BLR clouds be confined? Magnetic confinement is a likely possibility since the required magnetic field is small, about 1G. Confinement by HIM

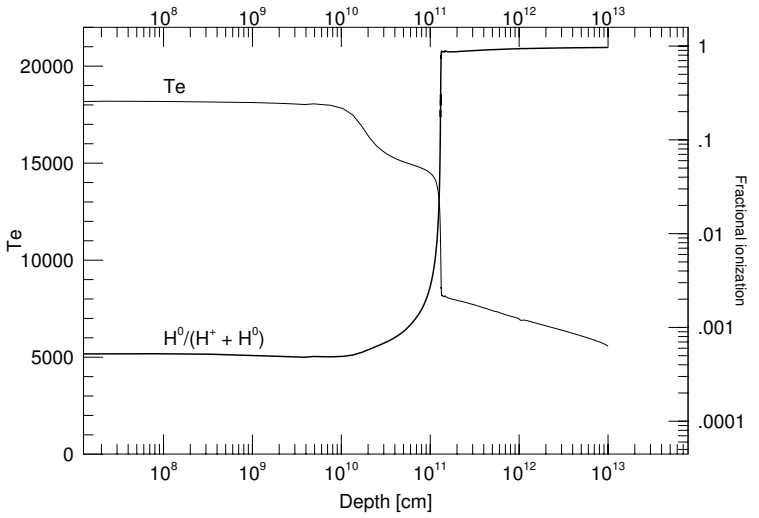

Fig. 7. The ionization and thermal structure of a 10^{23} cm^{-2} column density BLR cloud with $N_H = 10^1$ cm^{-3} exposed to a "typical" AGN SED at a distance which results in $U(hydrogen) = 0.01$.

is more problematic for various reasons. The required HIM density can be estimated from the assumed density and temperature of the BLR gas and from the requirement of pressure equilibrium. This gives $N_{HIM} \sim 10^7$ cm^{-3} for a Compton temperature of $\sim 10^7$ K. The dimension of the BLR in the most luminous AGN is of order 1 pc (see below). This gives a total Compton depth of more than unity for the HIM. The observational consequences are smearing of the central source variations and broad Compton scattering wings for all broad emission lines. This is generally not observed in AGN. There are, however, relativistic processes that can raise the HIM temperature beyond its Compton temperature. Such a relativistic HIM may still provide the required confining pressure.

How many high density clouds are required to produce the observed broad line profiles? Given the gas typical velocity, and the fact that individual confined clouds are likely to emit lines with a typical width of 10 km s^{-1}(roughly the sound speed in the gas), we can estimate the number of clouds required to produce the symmetrical and smooth profiles observed in many cases. The number is very large, of order 10^{6-8}. This raises serious questions about the formation and destruction of the clouds and possible collisions among clouds. A possible way out is to invoke internal turbulent motion that exceeds the sound speed by an order of magnitude or so. This results in a much broader single-cloud profiles and can alleviate some of the difficulties.

There are numerous studies about emission line intensities, broad line profiles, line variability and their correlation with continuum variations (see B.

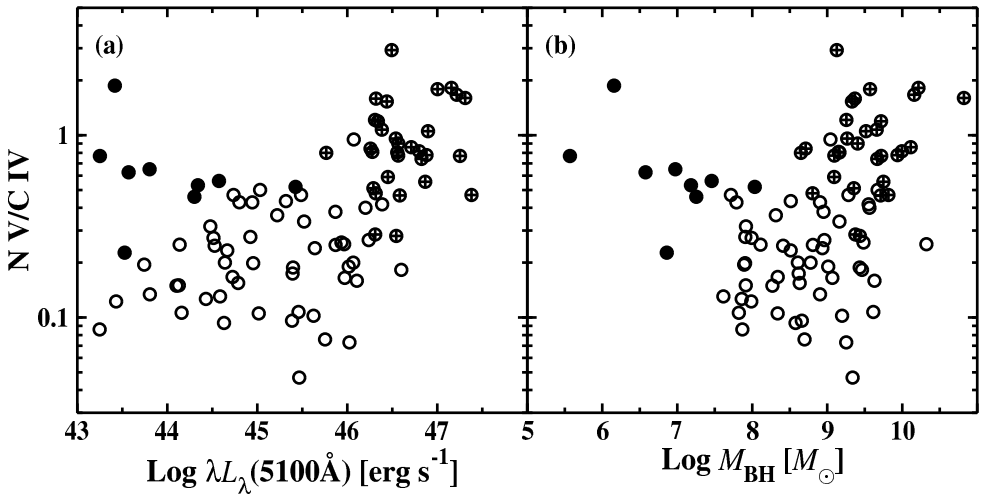

Fig. 8. Broad line region metallicity measure from NV/CIV as a function of luminosity and BH mass (from Shemmer et al et al. 2004).

Peterson contribution). Of particular interest are several recent papers that make use of the fact that BH mass and accretion rate can now be measured for a large number of sources using the reverberation mapping results. This enables a more physical insight into the BLR physics. Out of the large number of diagrams and correlations discussed in the literature I show here only a few addressing the issue of metallicity.

As explained, the gas metallicity in the BLR can be estimated from the N V λ1240/C IV λ1549 line ratio. Given known luminosity, BH mass and accretion rate (i.e. L/L_{Edd} one can search for the dependence of metallicity on one of those measures. Figs. 8 and 9 show several potential correlations for a relatively small sample of about 80 AGN. The reason for the small sample size is the fact that in low redshift sources, the above line ratio must be measured by HST and this is done one source at a time. Thus multi-object spectroscopy cannot help. As evident from the diagram, there are significant correlation of metallicity with all three variables if high-z high-L sources are considered. However, the correlation with BH mass and source luminosity weakens considerably when low luminosity cases are considered. In this case, the only significant correlation is with the normalized accretion rate, L/L_{Edd}.

A serious challenge to BLR models is to simulate *several* emission line intensities as they vary in response to the varying ionizing luminosity. This requires mapping all line emission sites and combining reverberation mapping studies (see Peterson's contribution) with a specific model for the cloud distribution (above equations). One such attempt, applied to the best studied case, NGC 5548, is shown in Fig. 10. It demonstrates that some observed emission line variations are well explained by the cloud model (i.e. a specific chosen distribution with specific values of s, p, and initial column density) but others, most notably the low ionization line of MgIIλ2800Å, are not in agreement with

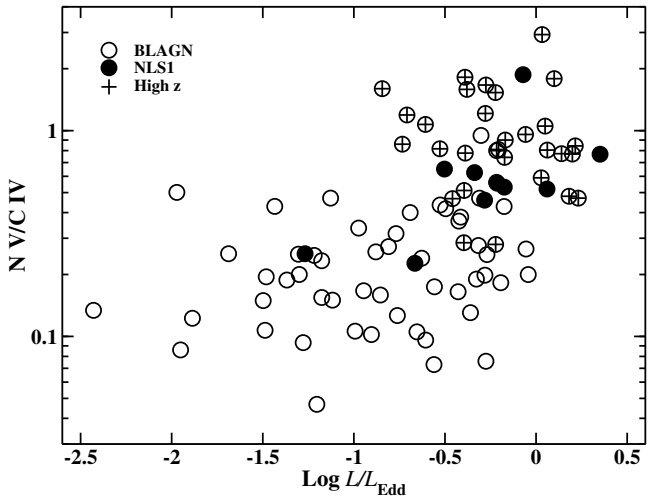

Fig. 9. Broad line region metallicity measure from NV/CIV as a function of L/L_{Edd} (from Shemmer et al et al. 2004).

the observations. This is likely to be the result of either wrong assumptions about the gas distribution in the outer part of the nucleus or, more likely, some missing physics in the modelling of low ionization lines.

Finally we comment of the more recent studies of BH mass and accretion rates in large AGN samples. These studies use RM results to measure 'single epoch" (see B. Peterson review) masses and accretion rates for many thousands of AGN. The example shown in Fig. 11 summarizes those properties for $\sim 10,000$ SDSS GN with $z \leq 0.75$. The study shows that smaller BHs accrete faster in the local universe, BH of all masses accrete faster at higher redshifts and the population accretion rate goes up with z in a slope which is similar to the SF slope, at least for small z.

3.2 The narrow line region

Next we consider smaller column density ($\sim 10^{20-21}$ cm^{-2}) low density ($\sim 10^4$ cm^{-3}) clouds situated at a location where $L/4\pi r^2 \simeq 10^2$ erg s^{-1} cm^{-2} (about 3 kpc for a very luminous AGN). We also assume a smaller covering fraction, of order 0.01-0.1. The ionization parameter for this gas is similar to the one obtained for the BLR and the typical velocity, assuming a bound system, 500 km s^{-1}.

The physical conditions in this larger region are considerably different from those in the BLR, despite the very similar level of ionization. First, the column density in some of the clouds is small enough to be optically thin in the hydrogen Lyman continuum. Under such circumstances, the radiation pressure force may be important and the line profiles may include a non-gravitational

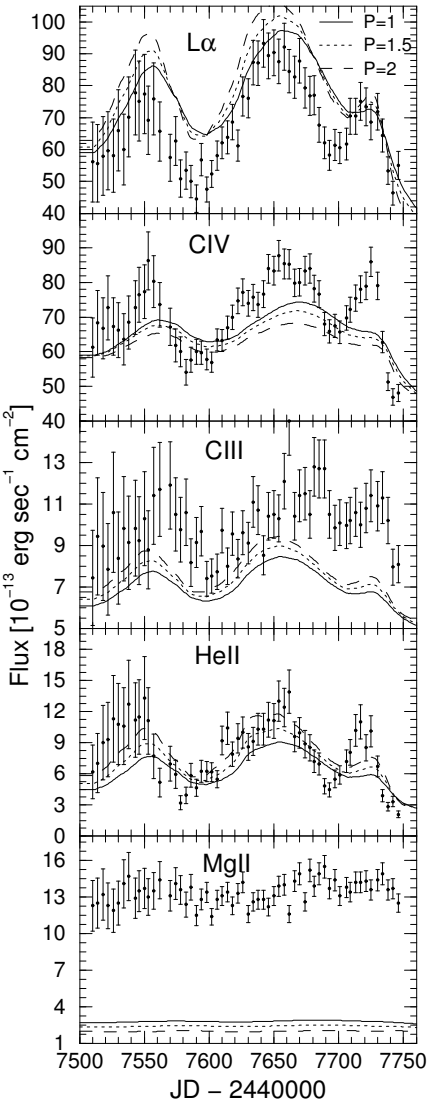

Fig. 10. Model fit to the variable emission line intensities in NGC 5548 (from Kaspi & Netzer 1999

components. Optically thin gas is, on average, more ionized than optically thick gas of the same ionization parameter. This will show in the spectrum of the gas. Confinement may not be an important issue since the life time of such large clouds is rather long. The EW of the emission lines is considerably smaller than that of the broad lines because of the smaller covering factor and the smaller Lyman continuum opacity.

The observed spectrum of this component includes intense forbidden lines, because of the low densities. This shifts the line cooling balance in such a way that the semi-forbidden and permitted lines are relatively weaker. Another group of lines that are predicted to be intense in the innermost part of this region are coronal lines, produced by fine-structure transitions and observed

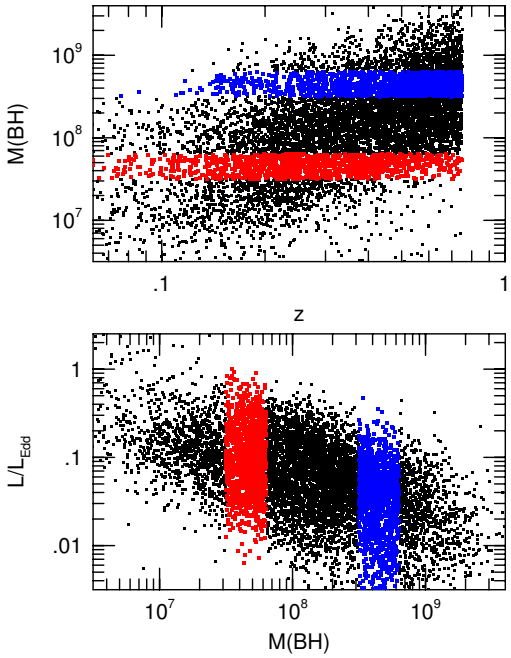

Fig. 11. Population properties of $\sim 10,000$ $z \leq 0.75$ SDSS AGN (after Netzer and Trakhtenbrot 2007). The diagram illustrates the dependence of BH mass on redshift (top) and the dependence of normalized accretion rate on BH mass (bottom). The various colors (shades) mark the locations of two groups of sources with BH masses at around $10^{7.5}$ and $10^{8.5}$ $M_{\odot}$.

mostly in the infrared. The region producing such a spectrum qualifies for the name "narrow line region" (NLR).

3.2.1 The narrow line spectrum and diagnostic diagrams

The NLR spectrum is perhaps the best studied AGN feature. optical-UV spectra, from the ground and space, have been obtained for numerous sources, occasionally in a spatially resolved manner. Line profiles have been investigated in great detail and IR spectroscopy enabled the measurement of many very high excitation lines (so called "coronal lines") that are prominent in this part of the spectrum. Fig. 3.2.1 shows one example of a Seyfert 2 galaxy. Focusing on type-II sources gives the clear advantage of avoiding the complication of separating broad and narrow line components in several permitted lines. This is based, of course, on the assumption that the NLR is identical in the two classes of sources.

A very useful way to investigate the physical conditions in the NLR is to construct diagnostic diagrams that are made by plotting various line ratios

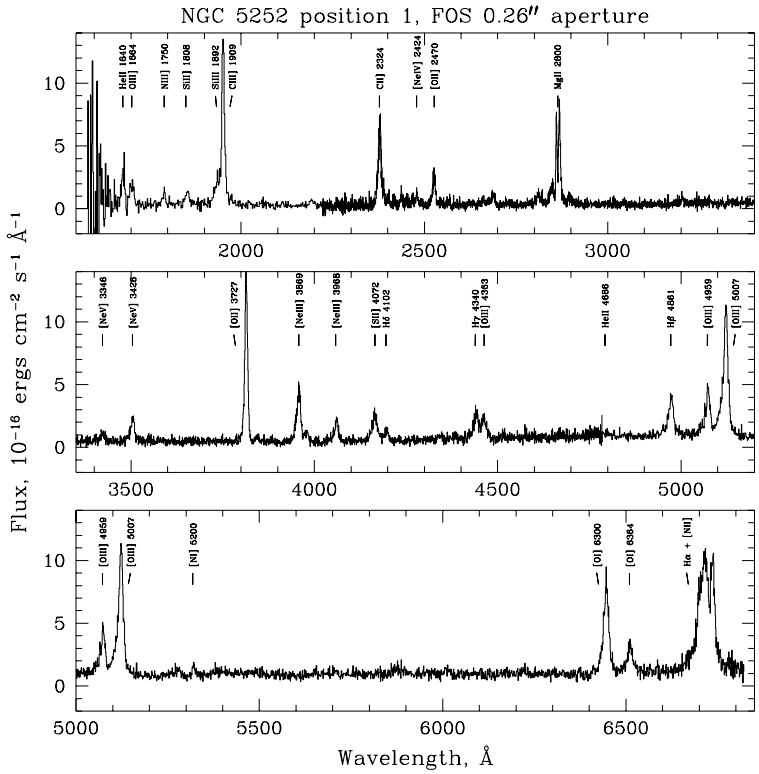

Fig. 12. A spectrum of a low luminosity type-II AGN (the Seyfert 2 galaxy NGC 5252)

against each other. This has been proven to give insight about the level of excitation of the gas (the ionization parameter), the gas metallicity and perhaps also the reddening. With present day large samples, like the SDSS with many thousands of spectra, one can use such diagrams to investigate the population properties in various way. Fig. 13 shows one such example that has been used to separate star-forming galaxies from AGN using the very different SEDs that ionized the gas in those sources.

3.3 Dust and reddening

Dust is a common ingredient in all astrophysical environments counting gas with a large enough metallicity. The obvious exceptions are very highly ionized plasmas heated by fast shock waves and regions very close to strong radiation sources where dust grains are too hot to survive. Thus, dust is likely to be present in various parts of AGN and in particular in their line emitting regions. Such dust will scatter and absorb some of the ionizing and non-ionizing radiation, will re-radiate the observed energy at infrared wavelengths and will modify the observed spectrum in various different ways (for more discussion

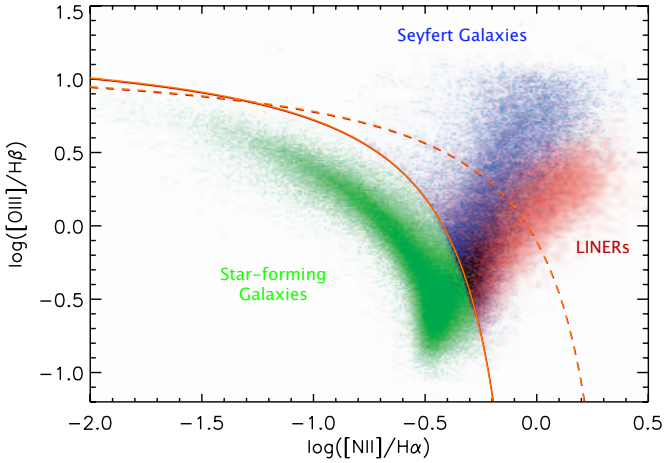

Fig. 13. The spread of various types of emission-line galaxies in an SDSS-based line ratio diagnostic diagram that uses four strong optical emission lines, [OIII] λ5007Å, [NII] λ6583Å, Hα and Hβ. The line ratios distinguish galaxies that are dominated by ionization from young stars (starburst galaxies), from those that are ionized by a typical AGN SED. The curves indicate empirical (solid) and theoretical (dashed) dividing lines between AGN and star-forming galaxies (Courtesy of B. Groves).

see Elitzur's contribution).

Most of the important dust properties are well explained by considering a single spherical dust grain, of radius a, situated a distance r from a radiation field L_ν. The grain is fully exposed to the radiation and all its emitted radiation can freely escape. The dust absorption cross section is Q_ν and its emissivity coefficient, assuming a black body source function, is $Q_\nu B_\nu$. The radiation absorbed by the grain is therefore

$$\frac{\pi a^2}{4\pi r^2} \int_0^\infty Q_\nu L_\nu d\nu \tag{51}$$

and the resulting grain emission is

$$4\pi a^2 \int_0^\infty \pi Q_\nu B_\nu(T_g) d\nu \,, \tag{52}$$

where T_g is the grain temperature. Since grain heating is given by eqn. 51 and grain cooling by eqn. 52, equating the two can be used to numerically solve for the grain equilibrium temperature, T_g.

For a grain situated inside a gas cloud, the incoming radiation is attenuated by gas and dust absorption inside the cloud. This makes the grain heating less efficient and requires an additional factor of $e^{-\tau_\nu}$ in eqn. 51. Such a grain is also heated by the radiation of other grains and by the diffuse gas radiation.

A simple (not very accurate) method to account for this effect is to use an escape probability formalism and multiply eqn. 52 by a term that takes into account the absorption of the emitted radiation by dust on the way out. This makes grain cooling less efficient and roughly accounts for the heating by the internally produced radiation assuming it is mostly due to dust.

A simple expression for the grain temperature can be derived by noting that most of the absorption takes place in the UV, where the absorption cross section is the largest, and most of the emission is in the IR, because of the expected value of T_g. For most known grains, the UV absorption cross section depends little on frequency and the IR absorption cross section, and hence emissivity, can be described by $Q_\nu \propto \nu^\gamma$ where the index γ depends on the size and the composition of the grain and is in the range of 0–2. For example, for large graphite grains $\gamma \simeq 0$ and for typical silicate grains $1 \leq \gamma \leq 1.5$. Using those notation we obtain the following expression for the grain equilibrium temperature,

$$T_g^{(4+\gamma)} = A \frac{L_{46}}{r_{pc}^2} \ , \tag{53}$$

where L_{46} is the integrated source luminosity in units of 10^{46} erg s^{-1}. The constant A depends on grain size and composition since both determine the value of γ. For an AGN with $L_{46} = 1$ and an intermediate size graphite grain at a distance of $r_{pc} = 1$, $A \simeq 1500\,\mathrm{K}$.

The properties of ISM dust in the Galaxy are normally specified by the fraction of metals in the dust phase (depletion), the particle size distribution and the other specific dust properties like grain shapes and composition. Graphitic dust and silicaceous dust are common in many dusty environments and were extensively studied in astronomical objects and in the laboratory. A commonly used composition, (so called "MRN composition", after the work of Mathis, Rumpl and Nordsieck) is made of graphite, enstatite, olivin, silicon cabide, iron and magnetite with a size distribution covering the range of 0.005–0.25 μm. It beautifully reproduces the observed galactic extinction curve given the assumed optical properties (absorption and scattering cross sections) and a size distribution of the form

$$\frac{dn(a)}{da} = k_d a^{-\alpha} \ . \tag{54}$$

For silicate and graphite grains, the index α is of order 3.5. The minimum grain size is determined by various destruction processes, such as photodestruction and the largest size is determined by the growth process of the grains (condensation and sticking). In galactic environment, $a_{min} < 0.01\mu$m but in AGN environment, some of the smallest grains may not survive because of the strong

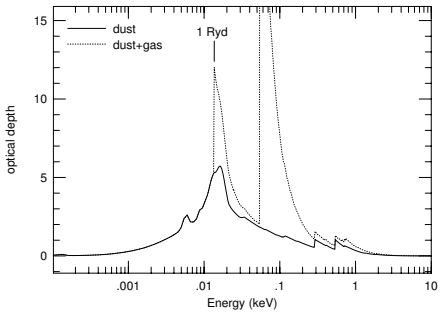

Fig. 14. Optical depth due to dust (solid line) and the combined dust and gas opacity (dotted line) for a $10^{21.5}$ cm^{-2} column density cloud with Galactic dust-to-gas ratio and MRN type dust. The ionization parameter chosen for this example result in similar gas and dust contribution to the the total opacity over the Lyman continuum wavelength range.

radiation field. The largest size is estimated to be about 0.3μm. Finally, the constant k_d in eqn. 54 depends on the dust-to-gas ratio and hence on the depletion of the heavy elements onto dust grains.

An additional important property is the dust sublimation temperature, T_{sub}, which is the maximum temperature attained by the grain before it evaporates. Laboratory and theoretical studies suggest that for graphite grains, $T_{sub} \simeq 1800\,\mathrm{K}$ while for silicate grains $T_{sub} \simeq 1400\,\mathrm{K}$. These numbers can be put together to derive a "sublimation radius", R_{sub}, which is the minimum radius where a grain of a certain composition can survive the central radiation field without evaporating. In general, smaller grains have larger γ and thus a larger temperature for a given radiation intensity. The result is that larger grains survive at smaller distances and there is a range of a factor ~ 3 in sublimation distances for different grains. Averaging over ISM-type grain size and composition, one obtains a typical value for AGN which is,

$$R_{sub} \simeq 0.5 L_{46}^{1/2}\,\mathrm{pc}\,. \tag{55}$$

Reverberation mapping of the BLR show that the mean $R_{\rm BLR}$ as determined by the emissivity of the Hβ line is

$$R_{BLR} \simeq 0.35 L_{46}^{0.6\pm0.1}\ pc\,. \tag{56}$$

Evidently, $R_{sub} \simeq R_{BLR}$ which suggests that there is a natural boundary to a dust-free BLR. Since dust is such a common component in all known HII regions, it is possible that almost the entire volume of the nucleus, from just outside the BLR to the outer edge of the NLR, is filled with dust.

There is clear observational evidence for dust outside the BLR from two types

of independent observations. First, IR monitoring of several near-by AGNs, mostly in the K band, clearly show reverberation of the light in this band relative to the light in the UV-optical continuum. The K-band emission is interpreted as dust radiation in the innermost part of the dusty AGN region (or the dusty torus - see later). The source of heating for this dust is the variable central continuum source and the time lag between the two bands can be used to calculate an empirical sublimation radius. This number seems to be in good agreement with the estimate given in eqn 55.

Another indication comes from searching for dust emission between the broad and the narrow emission line regions. There are several nearby sources where spatially resolves IR imaging detect such emission all the way down to a few pc from the center. The clearer signature is emission in the 10–20 μm range which is most likely due to the strong silicate dust emission features. Such a search can also be done in far away sources since the silicate features can be used to obtain the dust temperature and thus, from eqn 53, the distance to the region in sources whose optical-UV radiation is known. Studies of this type reveals the existence of "warm" ($T_g \sim 250\,\mathrm{K}$) dust in several high luminosity AGNs. The typical distance in this case is roughly 100-200 times R_{bub} i.e., way outside the BLR but not quite in the range where most narrow line emission is produced (which is another factor of about 10 further away).

The presence of dust in the gas producing the observed narrow line emission can substantially change its level of ionization and line emissivity. Such dust competes, effectively, with the ionization of the gas because of its large absorption cross sections at all wavelengths larger than about 0.02μm. The fraction of Lyman continuum photons absorbed by the dust, relative to those absorbed by the gas, depends on N_{dust}/N_{H^0}. For ionized gas with $N_{H^+} > N_{H^0}$ this is proportional to $U(\mathrm{hydrogen})$ since

$$\frac{N_{dust}}{N_{H^0}} \propto \frac{N_{gas}}{N_{H^0}} \simeq \frac{N_{H^+}}{N_{H^0}} \propto U(\mathrm{hydrogen})\,. \tag{57}$$

Therefore, dust is more efficient in attenuating the ionizing radiation in highly ionized gas, where it absorbs a larger fraction of the photons capable of ionizing hydrogen. The different ionization structures of dusty and dust-free environments are illustrated in Fig. 15 and 16.

Because of its large cross section, dust is also subjected to large radiation pressure force which is then delivered to the gas through the efficient charge coupling of the two components. In fact, the radiation pressure acceleration due to dust can be orders of magnitude larger than the acceleration given to the gas. This raises the interesting possibility that the internal pressure structure of the cloud is determined by the external radiation field through pressure balance. Since outside such dusty clouds $a_{rad}(r) \propto L/r^2$ and inside

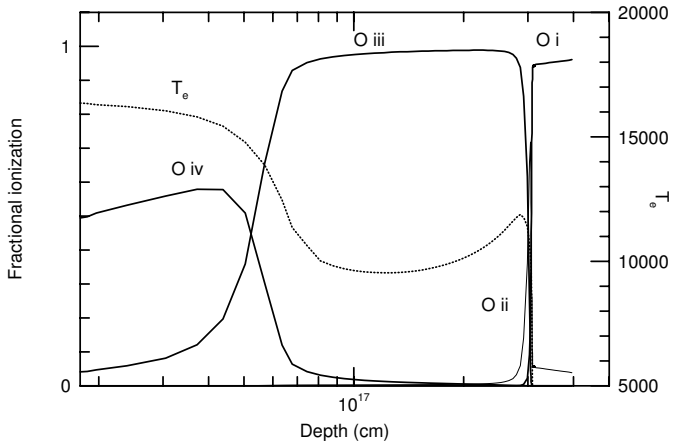

Fig. 15. The ionization and temperature structure of a constant density dust-free gas cloud exposed to a typical AGN ionizing continuum. In this case $N_H = 10^4$ cm^{-3} and U(hydrogen) = 0.03.

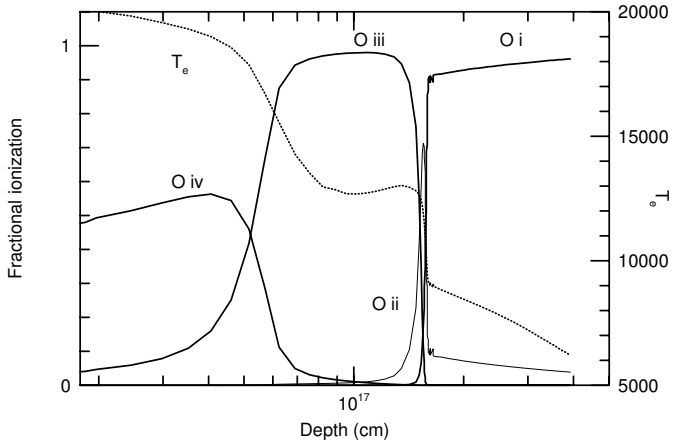

Fig. 16. Similar to Fig. 15 except that galactic type dust with the galactic dust-to-gas ratio is assumed to be present. Note the large reduction in the dimension of the ionized region and the increase in electron temperature mostly because of the depletion of carbon and oxygen that provide the strongest cooling lines.

the cloud $P_g \propto N_H$, we find that for all such clouds $L/r^2 \propto N_H$. The conclusion is that for dusty ionized gas

$$U \propto L/N_H r^2 = const. \tag{58}$$

This fixes both the absolute value of the ionization parameter and the fact that it is location independent. NLR models based on this idea are quite successful in reproducing the observed NLR spectrum while providing the physical jus-

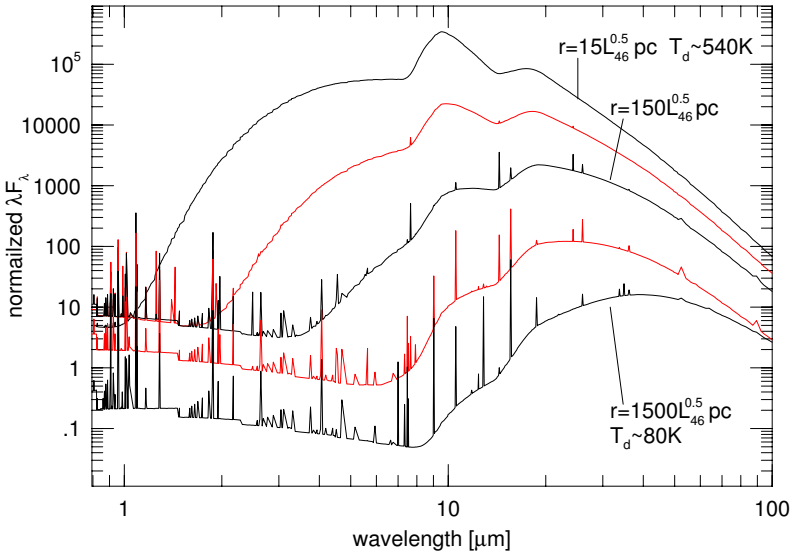

Fig. 17. The spectrum produced by dusty AGN clouds situated at various distances, as marked, from a luminous central source with $L = 10^{46}$ erg s^{-1} ($L_{46} = 1$). The calculations assume a gas density of 10^4 cm^{-3} and a column density of $10^{21.5}$ cm^{-2}. Galactic dust-to-gas ratio is assumed with dust properties and depletion factors similar to what is observed in Galactic HII regions. The assumed gas density determines the ionization parameter at the given distance thus clouds at the same location but smaller (higher) gas density will show spectra of more ionized (less ionized) emission line gas (adopted from calculations by B. Groves).

tification for the specific observed value of U(hydrogen). Such models require that $U \geq 10^{-1.5}$ at the illuminated face of the cloud since only for such U the dust opacity dominates over the gas opacity (see Eq. 57). Obviously, the effective ionization parameter inside the gas, where most line emission is taking place, is smaller because of the increasing neutral hydrogen opacity. An obvious shortcoming of the model is the lack of explanation for the absence of gas at the locations where $U < 10^{-1.5}$ at the illuminated face. In particular, one can imagine a situation where there is a large density range at each location and only those clouds with density below a certain value (and hence ionization parameter above a certain value) produce the "typical" (to this model) dusty-gas spectrum.

Finally, dust has been suggested to be present even in the most luminous AGN and to affect the luminosity and shape of the non-stellar continuum and the broad emission line ratios. Such dust is difficult to observe because of the unknown shape of a pure, un-extincted AGN continuum and the large uncertainties on the intrinsic broad emission line ratios. It is clear that such dust, if it exists, does not show the 2175Å dust feature observed in many

galactic sources. This is not surprising since the AGN environment is so different that the grain size distribution, and even the dust composition, may be very different from those of typical galactic dust. Some interesting ideas include dust with relatively little amount of very small grains. This will result in a grey extinction at short wavelengths which is supported by some observations. More extreme scenarios suggest diamond dust with steep extinction curve near the Lyman limit and hardly any absorption or scattering at much longer wavelengths.

3.4 The highly ionized gas

Next consider the region between the NLR and the BLR, 0.1–10 pc from the center. Assume intermediate to large (10^{21-23} cm^{-2}) column density gas and a density such that the ionization parameter is 10–100 times larger than in the BLR. For this gas $U(\mathrm{oxygen}) \sim 0.02$ thus we expect strong absorption and emission features in the X-ray part of the spectrum. Similar temperatures and levels of ionization can be found in gas with a much lower density which is distributed inside the NLR. A proper name for such a component is the *highly ionized gas* (HIG). In the X-ray literature is is often called "warm absorber". For scaling purposes we note that the density of a typical HIG cloud is

$$N_{HIG} \simeq 2 \times 10^4 U(\mathrm{oxygen})^{-1} L_{44}(\mathrm{oxygen}) R_{\mathrm{pc}}^{-2} \ \mathrm{cm}^{-3} \ , \tag{59}$$

and its mass is

$$M_{\mathrm{HIG}} \simeq 10^3 \, N_{22} C_f R_{\mathrm{pc}}^2 \ M_\odot \, , \tag{60}$$

where N_{22} is the hydrogen column density (assuming solar composition) in units of 10^{22} cm^{-2} and L_{44}(oxygen) the 0.54–10 X-ray luminosity in units of 10^{44} erg s^{-1} (for low luminosity AGN, like NGC 5548 and NGC 3783, $L_{44}(\mathrm{oxygen}) \simeq 0.05$ and for high luminosity quasars $L_{44}(\mathrm{oxygen}) \simeq 1$).

Modern X-ray observations of type-I AGN show the clear signature of such gas. The strongest spectral features are numerous absorption lines of the most abundant elements, strong bound-free absorption edges due mostly to O VII and O VIII, and several emission lines. Perhaps the best spectrum of this type (correct to 2004) is a 900 ks spectrum of NGC 3783 obtained by *Chandra* HETG. This spectrum was observed in two states of the source, high and low, that differs by about a factor of 1.5 in flux of the hard X-ray continuum. Part of the low-state spectrum is shown in Fig. 18.

The X-ray spectrum of type-II AGN is completely different, because of the large obscuration in this type of sources. It shows prominent X-ray emission

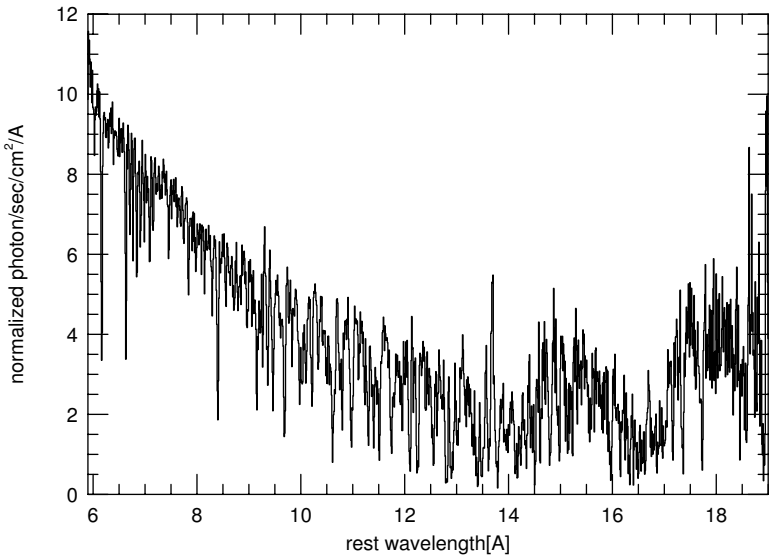

Fig. 18. Part of the low-state spectrum of NGC 3783 observed by *Chandra* in 2002. Some 60 X-ray lines were identified in this part of the spectrum.

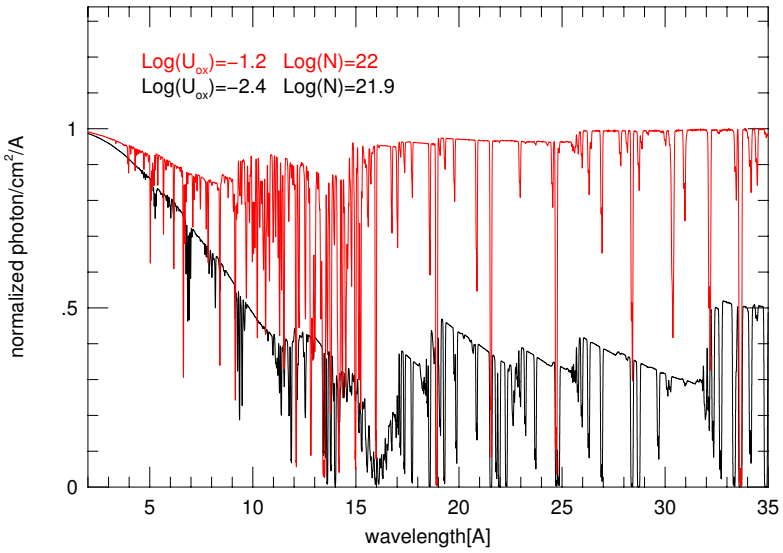

Fig. 19. Two of the three components required to model the low-state spectrum of NGC 3783 shown in Fig. 18.

lines that indicate similar properties to the gas producing the strong absorption in type-I AGN. In some of the sources the X-ray emitter is resolved and its dimension can be directly measured. This indicates X-ray emission region of several hundred pc in diameter. It is not yet clear whether the type-I absorbers are of similar dimensions. In fact, some well studied cases indicate much smaller absorption regions.

3.4.1 HIG outflows

The HIG gas is transparent to the UV and soft X-ray radiation and is thus subjected to a strong radiation pressure force, compared with the opaque BLR gas. This can results in mass outflow from the nucleus. Such outflows have been observed in several well studied cases and it is interesting to consider their affects on the general AGN environment.

The mass outflow rate of the HIG can be inferred from its observed velocity and from the known (or guessed in some cases) location. It is given by

$$\dot{M}_{\rm HIG} = 4\pi r^2 C_f \rho v_{\rm HIG} \epsilon_{\rm HIG} \tag{61}$$

where C_f is the covering fraction and $\epsilon_{\rm HIG}$ the filling factor of the HIG. The associated dynamical time is $r_{\rm HIG}/v_{\rm HIG}$ which is of order a thousand years for HIG at several pc from the center and outflow velocity of several hundred km s^{-1}. Such outflows can interact with the NLR gas and disturb or modify the gas distribution at that location. It can also reach the ISM and the galactic halo on time scales of several million years with important consequences to the overall cooling and energy output to the inter-galactic medium.

3.4.2 Associated UV absorbers

Are X-ray absorption lines the only signature of HIG at the above mentioned location? The answer to this question depends on the level of ionization and the column density of the gas. Large columns and low ionization parameters can result in HIG whose less ionized species may well be C IV, N V, O V and O VI. Relatively small column density of such ions along the line of sight can produce strong UV absorption lines with typical widths similar to the widths of the X-ray absorption lines. Interestingly, some of the ions, e.g. O VI, show both UV and X-ray lines which can be compared to test the idea that the UV and X-ray absorption lines originate in the same moving gas component. Fig. 20 shows a typical example of UV absorbers in an AGN whose X-ray spectrum shows the clear absorption signature of HIG.

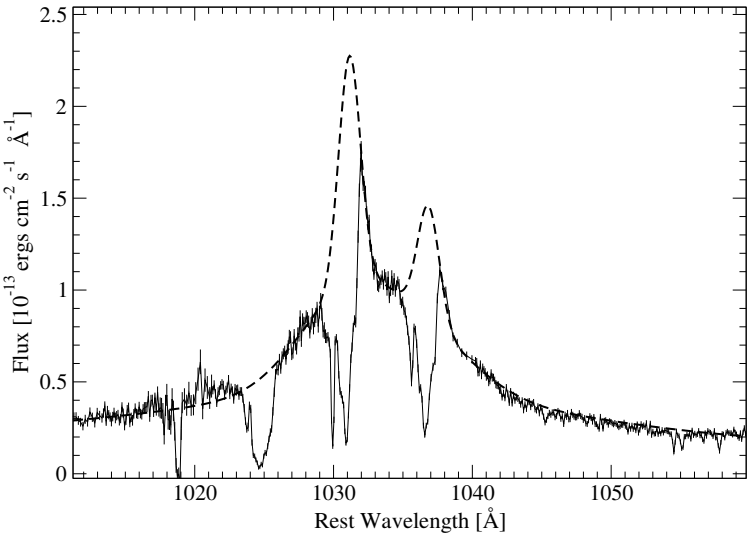

Fig. 20. The FUSE spectrum of the quasar MR 2251-178 showing narrow OVI absorption lines superimposed on emission lines of the same ion. The derived outflow velocities are in the range 300–600 km s^{-1}. The source also shows time-dependent X-ray absorption lines.

3.5 The torus

We next consider a region of size 1–100 pc located around the central BH with density of $10^4 - 10^6$ cm^{-3} and extremely large column density, 10^{25} cm^{-2} and even larger. We assume a flat geometry i.e. a torus or a collection of large column density clouds moving in a plane.

The above structure covers such a large range in radii that we expect a large range in physical conditions. Far from the center, at 10 or even 100 pc, the gas is very optically thick with very low temperature. Only the hard X-ray radiation can penetrate that far and even those photons are limited to a few Compton depths. The conditions must be similar to those in molecular gas in the galaxy. Such regions are likely to contain large amount of dust. Their spectral signature are infrared emission and absorption with strong dust features.

The inner part of such a structure is exposed to the central radiation field. The temperature and ionization of this part depend on the ionization parameter. Using the previously defined L_{44}(oxygen), and assuming a typical X-ray SED, we get

$$U(\text{oxygen}) \simeq 0.2 L_{44}(\text{oxygen}) r_{pc}^{-2} N_5^{-1} \ , \tag{62}$$

where $N_5 = N_H/10^5\,\text{cm}^{-3}$ and r_{pc} the distance to the inner wall in pc. Assume for example $L_{44}(\text{oxygen}) = 0.1$ (intermediate luminosity AGN), $r_{pc} = 1$ and

$N_5 = 0.1$. This gives $U(\text{oxygen}) = 0.2$. This would produce strong high ionization X-ray lines from the torus cavity. In particular, low, intermediate and high ionization iron K_α lines are expected to show as a clear signature of such a structure. Because of the huge column density, such a wall is a very efficient "X-ray reflector" which will scatter and reflect the incident X-ray continuum radiation. Finally, we note that the inner parts of such a torus are a likely gas reservoir for both X-ray driven winds and accretion onto the central BH.

4 Conclusions

The physics of ionized gas in AGN is govern by a few fundamental principles: Gas is present on all scales, from a fraction of a pc to a very large distance (several kpc for NLRs in high luminosity AGN). The central strong radiation field is the main, perhaps the only ionization and heating source for the gas. Gas dynamics in some regions is almost completely governed by the BH mass. Some components are however affected by radiation pressure force due to the central source (HIG and wind outflows) and/or the stellar mass (extended NLRs). Variability of the central source drives the variability of the broad emission lines. There are claims that such variations are also responsible for the observed variations in the spectrum of X-ray emitting outflowing gas. There are indications of super-solar metallicity especially in the BLR of high luminosity, fast accreting AGN.

5 References

The following list cannot do justice to hundreds of authors that published thousands of papers about AGN gas and physical processes. The purpose is to provide a convenient starting points for further reading about some of the topics discussed in this review. Therefore, the main emphasis is on comprehensive reviews rather than on specific papers.

General reviews and books that cover the topics and the physical processes discussed here are:

(1) Netzer, H. 1990, in "Active Galactic Nuclei" (SAAS-FEE 1990)
(2) Peterson, B., "Introduction to Active Galactic Nuclei" (Cambridge University Press)
(3) Krolik, J.H., "Active Galactic Nuclei" (Princeton Series in Astrophysics)
(4) "Interpreting Astronomical Spectra" (D. Emerson, Wiley).
(5) Ferland, G., 2003, AnnRevAstAp , 41, 517
(6) Paerels, F. B. S. & Kahn, S. M., 2003, AnnRevAstAp 41, 291

(7) Osterbrock, D & Ferland, G., "Astrophysics of Gaseous Nebulae and Active Galactic Nuclei" (2005, University Science Books)

Dusty NLRs are discussed in numerous publications. The recent suggestion of a radiation pressure dominated NLR is discussed in Dopita et al. (2002, ApJ, 572, 753), Groves et al (2004, ApJS, 153, 9) and several other papers by Groves, Dopita and Sutherland.

Hamann, F. & Ferland, G. (1999, AnnRevAstAp, 37, 487) is the main source for BLR metallicity.

Shemmer et al. (2004 ApJ 614, 547) is a more recent study of BLR metallicity.

The idea of the LOC model is outlined in several papers by Baldwin, Korista and Ferland, e.g. ApJ, 487, 555 (1997).

A comprehensive review of HIG properties and the associated UV absorbers is given in Crenshaw, Kraemer & George (2003, AnnRevAstAP, 41, 117).

'The Starburst AGN Connection" (Aretxaga, Kunth & Mujica eds., 2000, World Scientific) is a useful collection of papers discussing, among other things, the physics of various AGN components.